Stabilization of dynamic microtubules by mDia1 drives Tau-dependent $A\beta_{1-42}$ synaptotoxicity

Xiaoyi Qu,[1] Feng Ning Yuan,[1] Carlo Corona,[1] Silvia Pasini,[1] Maria Elena Pero,[1,2] Gregg G. Gundersen,[1] Michael L. Shelanski,[1] and Francesca Bartolini[1]

[1]Department of Pathology, Anatomy and Cell Biology, Columbia University, New York, NY
[2]Department of Veterinary Medicine and Animal Production, University of Naples Federico II, Naples, Italy

Oligomeric Amyloid β_{1-42} (Aβ) plays a crucial synaptotoxic role in Alzheimer's disease, and hyperphosphorylated tau facilitates Aβ toxicity. The link between Aβ and tau, however, remains controversial. In this study, we find that in hippocampal neurons, Aβ acutely induces tubulin posttranslational modifications (PTMs) and stabilizes dynamic microtubules (MTs) by reducing their catastrophe frequency. Silencing or acute inhibition of the formin mDia1 suppresses these activities and corrects the synaptotoxicity and deficits of axonal transport induced by Aβ. We explored the mechanism of rescue and found that stabilization of dynamic MTs promotes tau-dependent loss of dendritic spines and tau hyperphosphorylation. Collectively, these results uncover a novel role for mDia1 in Aβ-mediated synaptotoxicity and demonstrate that inhibition of MT dynamics and accumulation of PTMs are driving factors for the induction of tau-mediated neuronal damage.

Introduction

The presence of amyloid plaques and hyperphosphorylated tau-loaded neurofibrillary tangles (NFTs) in the brain are invariant features of Alzheimer's disease (AD). There is compelling evidence that soluble oligomeric Amyloid β_{1-42} (Aβ) plays a critical neurotoxic and synaptotoxic role during the early stages of AD (Nimmrich and Ebert, 2009; Pozueta et al., 2013a), and it has been proposed that the microtubule (MT)-associated protein (MAP) tau mediates the effects of Aβ in dendrites and axons (LaFerla, 2010; Ittner and Götz, 2011; Mairet-Coello et al., 2013; Sherman et al., 2016; Wang et al., 2016). Hyperphosphorylation of tau decreases its binding to MTs, and multiple studies support a role for Aβ in up-regulating tau phosphorylation (Busciglio et al., 1995; Zheng et al., 2002; Zempel et al., 2010; Jin et al., 2011; Mairet-Coello et al., 2013; Muratore et al., 2014). It was thus initially hypothesized that Aβ overproduction causes neurotoxicity through destabilization of the axonal MT cytoskeleton as a result of accumulation of insoluble hyperphosphorylated tau. Alternatively, neuronal injury may originate through Aβ-mediated mislocalization of soluble hyperphosphorylated tau to dendritic spines (Zempel et al., 2010), where it induces loss of glutamate receptors (Hoover et al., 2010), PrP^C-mediated neurotoxicity by transporting Fyn kinase to dendritic spines (Ittner et al., 2010), and MT severing (Zempel et al., 2013). More recently, a role for pathological tau mutants and hyperphosphorylated tau has been further uncovered in presynaptic dysfunction (Zhou et al., 2017). Although these mechanisms may each contribute to synaptic injury and cell death in AD, the molecular nature of the link between Aβ and hyperphosphorylated tau remains poorly understood.

We hypothesized that a primary activity of Aβ is to activate pathways that alter MT behavior and/or tubulin posttranslational modifications (PTMs) associated with MT stability and that these changes trigger a cellular stress response that leads to tau hyperphosphorylation in an attempt to restore normal MT function. In support of this model, recent evidence has shown a neurotoxic role for Aβ in acute induction of tubulin polyglutamylation (Zempel et al., 2013) and acetylation (Tsushima et al., 2015) in hippocampal neurons. These are compelling results given the implication of tubulin PTMs in the ubiquitous regulation of MT plus end–tracking proteins (+TIPs), MAPs, MT motors (Janke and Kneussel, 2010; Janke and Bulinski, 2011; Janke, 2014; Chakraborti et al., 2016), and in the case of tubulin polyglutamylation, synaptic vesicle transport (Maas et al., 2009), MT severing (Lacroix et al., 2010), and Purkinje cell degeneration (Rogowski et al., 2010).

Emerging studies from several groups indicate that dynamic MTs, typically deprived of tubulin PTMs, play key roles

Correspondence to Francesca Bartolini: fb2131@cumc.columbia.edu

F.N. Yuan's present address is Loyola University Chicago, Maywood, IL.

S. Pasini's present address is Dept. of Ophthalmology and Visual Science, Vanderbilt University Medical Center, Nashville, TN.

Abbreviations used: +TIP, MT plus end–tracking protein; Aβ, Amyloid β_{1-42}; AD, Alzheimer's disease; APP, amyloid precursor protein; DIV, d in vitro; Glu MT, detyrosinated MT; IF, immunofluorescence; KO, knockout; LPA, lysophosphatidic acid; LTP, long-term potentiation; MAP, MT-associated protein; mEPSC, miniature excitatory postsynaptic current; MT, microtubule; NFT, neurofibrillary tangle; PTM, posttranslational modification; WB, Western blot.

The Rockefeller University Press
J. Cell Biol. Vol. 216 No. 10 3161–3178
https://doi.org/10.1083/jcb.201701045

in neuronal function. Dynamic MTs polymerize from dendritic shafts into spines, and signaling through NMDA receptors and local calcium entry regulate this process (Gu et al., 2008; Mitsuyama et al., 2008; Kapitein et al., 2010, 2011; Dent et al., 2011; Hu et al., 2011; Merriam et al., 2011, 2013). Invasion of dendritic spines by dynamic MTs can in return affect spine morphology and function by regulating myosin- and kinesin-paired cargo dynamics (Jaworski et al., 2009; McVicker et al., 2016). A critical role for dynamic MTs in presynaptic terminals has been highlighted in *Drosophila melanogaster* neuromuscular junction boutons in which reduced organization of the MT cortex loop and stabilization of presynaptic MTs cause the deficits in fly models of fragile X syndrome and hereditary spastic paraplegia (Zhang et al., 2001; Lu et al., 2004; Trotta et al., 2004). Indeed, presynaptic dynamic MTs are necessary to deliver synaptic vesicles and may further mediate storage and/or docking/fusion of vesicles at the active zone (Lepicard et al., 2014).

Thus, aside from their more conventional role in offering structural support to the neuron, MTs are fine regulators of neuronal homeostasis and synaptic function, and unwanted changes in MT dynamics and/or tubulin PTMs may be directly involved in the onset of neurodegenerative disease. Interestingly, biphasic fluctuations of tubulin detyrosination and corresponding MT instability/stability phases have been associated with memory formation and are disrupted in aging, suggesting a primary role for the regulation of MT dynamics and at least this tubulin PTM in the maintenance of synaptic plasticity (Uchida et al., 2014; Uchida and Shumyatsky, 2015).

Recently, we showed that Aβ induces stable detyrosinated MTs (Glu MTs) in NIH3T3 cells and primary neurons in a Rho-mediated manner (Pianu et al., 2014). In NIH3T3 cells, Glu MT induction by Aβ is the result of MT stabilization, is regulated by integrin signaling, and occurs through the activation of a pathway involving amyloid precursor protein (APP)/caspases and mDia1 (Pianu et al., 2014), a Rho effector and a member of the family of formins with independent roles on the actin and MT cytoskeletons (Bartolini and Gundersen, 2010; Chesarone et al., 2010). Thus, induction of stable MTs by Aβ appears to be mediated by the same pathway that leads to stable MTs in fibroblasts downstream of lysophosphatidic acid (LPA; Cook et al., 1998; Palazzo et al., 2001, 2004; Goulimari et al., 2005; Bartolini et al., 2016) and is initiated by the same APP/caspase/RhoA signaling cascade that causes loss of dendritic spines by Aβ in neurons (Huesa et al., 2010; Chacon et al., 2011; Lefort et al., 2012; Pozueta et al., 2013b).

In this study, we analyze the nature of Aβ-induced Glu MTs in hippocampal neurons and implicate the formin mDia1 in a pathway that stimulates synaptotoxicity through MT-dependent tau hyperphosphorylation.

Results

Aβ induces Glu MTs by stabilizing dynamic MTs in hippocampal neurons

We investigated whether Glu MTs induced by oligomer-enriched Aβ preparations in neurons (Pianu et al., 2014) resulted from an increase in MT stability. We found that synaptotoxic concentrations of Aβ induced a transient accumulation of both Glu and acetylated tubulins, two independent tubulin PTMs associated with MT longevity, suggesting that induction of Glu MTs by Aβ reflected an acute gain in MT stability rather than regulation of the enzymes that control tubulin detyrosination (Fig. 1, A and B). To assess MT stability directly, we measured residual MT polymer levels (βIII-tubulin staining) upon nocodazole-induced MT depolymerization and found a higher degree of MT resistance in Aβ-treated neurons than in controls (Fig. 1, C and D). We analyzed the mechanism of this MT stabilization by quantifying the behavior of EB3-EGFP comet movements in proximal dendrites and axons to measure MT plus end dynamics before and after acute Aβ treatment (Fig. 1, E–J; and Fig. S1). No significant change was observed in rescue/nucleation frequency (number of MTs switching from shrinkage to growth or newly formed MTs per unit area and time), comet density (number of comets per unit area and time), or growth rates in dendrites or axons of neurons treated with Aβ up to 8 h (Fig. S1). However, we detected a transient increase in comet lifetime and length of growth in dendrites treated with Aβ as a result of a ∼40% drop in catastrophe frequency, the rate at which dynamic MTs switch from growth to shrinkage and that in neurites is obtained by dividing the number of comets by the total duration of all growth events (Fig. 1, E and F; and Fig. S1 A; Stepanova et al., 2010). No significant change in catastrophe frequency was observed with vehicle or scrambled Aβ control (Fig. 1 H). Interestingly, a more severe (∼55% drop) and longer-lasting inhibition of catastrophe frequency (up to 6 h) was observed in axons (Figs. 1 G and S1 B). We tested whether the transient nature of this effect resulted from either desensitization of the neurons or loss of Aβ activity in cell culture (Zempel et al., 2013). We found that although in axons a second dose of Aβ did not significantly affect the kinetics and intensity of the response (Fig. 1 J), prolonged inhibition of catastrophe frequency in dendrites could be achieved by treating neurons with a second dose of Aβ (Fig. 1 I). However, as inhibition of MT dynamics occurred both in axons and dendrites and regardless of comet orientation (Fig. S1 A), the results suggest that Aβ inhibition of MT dynamics is not selective for either compartment. Because of the greater number of dendrites per neuron, we elected to limit the rest of our analyses to dendritic MTs.

In summary and in agreement with the observation that induction of modified tubulins lagged behind the rise in comet lifetime, these data suggest that Aβ acutely stabilizes dynamic MTs by inhibiting their catastrophe frequency.

Stabilization of dynamic MTs by Aβ is dependent on APP but not tau expression

Our previous work in nonneuronal cells, which are naturally deprived of tau expression, highlighted a role for APP in the initiation of a tau-independent pathway that leads to stable Glu MTs downstream of Aβ (Pianu et al., 2014). To test whether this was also true in neurons, we acutely interfered with tau expression by lentiviral-mediated silencing to avoid developmental compensation of MT behavior as revealed by lack of clear MT phenotype in tau-knockout (KO) neurons (Harada et al., 1994), and we examined the effect of Aβ on MT dynamics and stability. We found that significant depletion of tau expression (Fig. 2, A and B), which only modestly increased MT growth rates (Fig. 2 D), did not interfere with acute MT stabilization or inhibition of catastrophe frequency induced by Aβ (Fig. 2, C and D). To the contrary, loss of APP expression obliterated induction of MT stabilization and inhibition of dynamic MT behavior in APP-KO neurons treated with Aβ (Fig. 2, E–G).

These results argue that the acute changes in MT behavior caused by Aβ are independent of tau expression and suggest

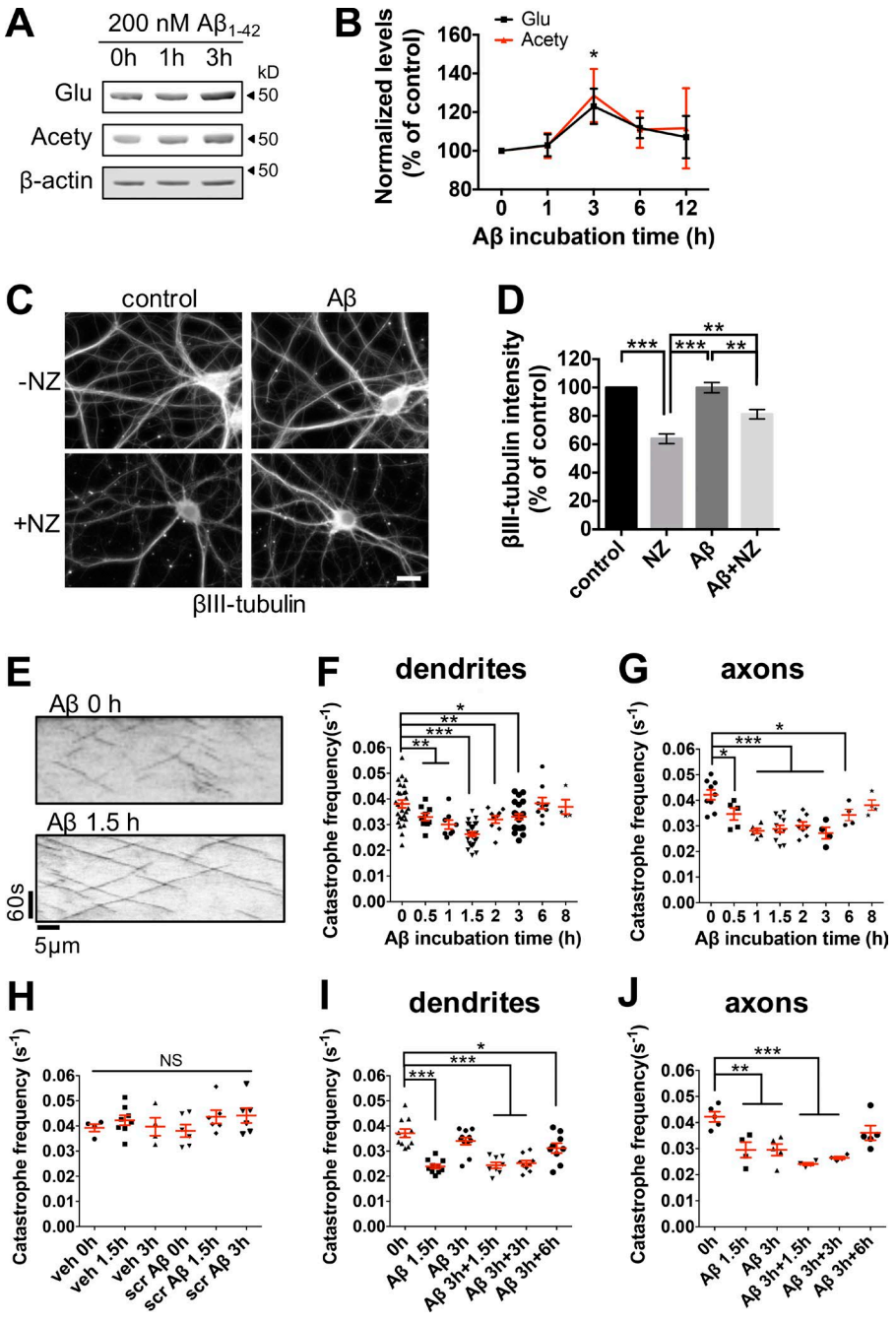

Figure 1. **Aβ stabilizes MTs by inhibiting MT dynamics in hippocampal neurons.** (A) WB analysis of detyrosinated (Glu) and acetylated (Acety) tubulin in cultured hippocampal neurons (18 DIV) treated with oligomer-enriched preparation of Aβ. (B) Time course of Glu and acetylated tubulin induction by Aβ. Data were normalized to β-actin levels. (C) IF of βIII-tubulin in hippocampal neurons (18 DIV) treated with Aβ for 1.5 h and incubated with nocodazole (NZ) 1 h before MT extraction and fixation. Control, vehicle. Bar, 20 µm. (D) Quantification of residual MT mass in major proximal neurites of neurons treated as in C. (E) Representative kymographs at 0 h and 1.5 h of incubation with Aβ. (F, G, I, and J) Time course of MT catastrophe frequency measured from EB3-EGFP comet movement in proximal dendrites or axons of hippocampal neurons (18 DIV) upon a single dose of Aβ (F and G) or a second dose at 3 h for increasing times (I and J). (H) MT catastrophe frequency before and after incubation with vehicle (veh) or scrambled (scr) Aβ peptide. Data in F–J are analyzed from 30–362 comets for each group. Data are shown as means ± SEM. *, $P < 0.05$; **, $P < 0.01$; ***, $P < 0.001$ by one-way ANOVA followed by Dunnett's multiple comparison test based on experiments (B, $n = 3$) or Tukey's multiple comparison test based on neurites (D, $n = 44–50$; F–J, $n = 4–27$).

that this APP-dependent MT pathway is conserved in neurons and possibly contributes to Aβ synaptotoxicity.

The formin mDia1 mediates stabilization of dynamic MTs and synaptotoxicity caused by Aβ

mDia1 is the main formin responsible for the generation and maintenance of stable Glu MTs downstream of Rho activation by LPA and Aβ in NIH3T3 cells (Palazzo et al., 2001; Goulimari et al., 2005; Pianu et al., 2014). We hypothesized that this function would be conserved in neurons and tested the role of mDia1 in the induction of stable MTs and inhibition of MT dynamics by Aβ using a commercially available formin inhibitor (SMIFH2; Rizvi et al., 2009). We first characterized the inhibitor alone in neurons (Fig. S2) and in NIH3T3 cells (Fig. S3, A and B) to evaluate its range of activity, and we confirmed its reversible inhibitory effect on MT stability as well as its independence from tau expression in neurons (Fig. S2, A–D). We found that even the lowest used dose of SMIFH2 (10 nM), which alone had no effect on MTs or Aβ internalization (Figs. 3 and S2, E–H), abrogated acute Glu MT induction and inhibition of MT dynamics caused by Aβ in neurons (Fig. 3, A–C). Formin inhibition was also sufficient to inhibit LPA or Aβ-mediated increases in stable Glu MTs in NIH3T3 cells (Fig. S3), confirming the convergence of these MT pathways in nonneuronal cells.

We then examined whether acute MT stabilization caused by Aβ represented a neuroprotective response or rather contributed to Aβ neurotoxicity. To this end, we analyzed the result of formin inhibition on the damage inflicted by Aβ on dendritic spine density and long-term potentiation (LTP; Fig. 4). We

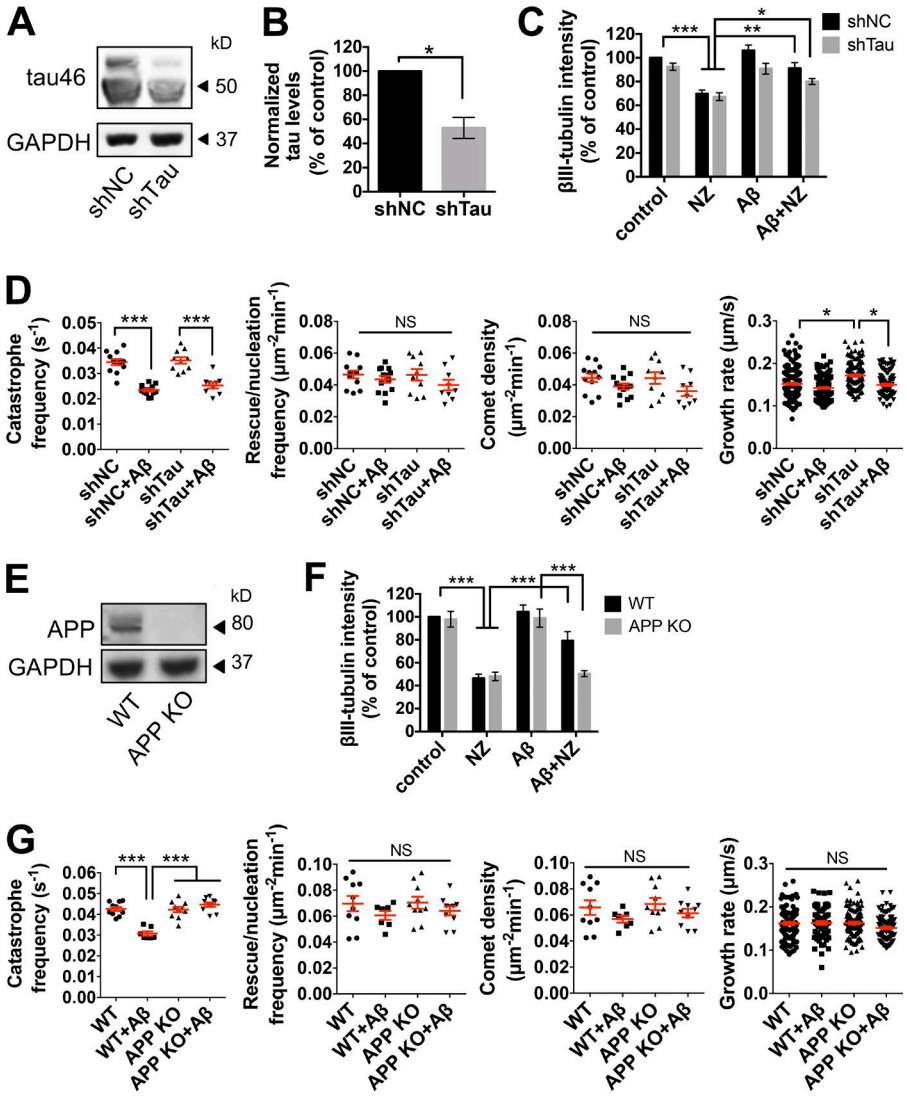

Figure 2. **Aβ inhibits MT dynamics independently of tau but not APP.** (A) WB analysis of total tau (tau46) levels in hippocampal neurons (19 DIV) treated with noncoding control (shNC) or shRNA against tau (shTau) lentivirus for 5 d. (B) Quantifications of tau levels normalized to GAPDH levels. (C) Quantification of MT stability (residual βIII-tubulin levels) in shNC- or shTau-infected neurons (19 DIV). Control, vehicle. (D) EGFP-EB3 analysis of MT dynamics parameters in hippocampal neurons (19 DIV) infected with shNC or shTau lentiviruses for 5 d ± Aβ (200 nM, 1.5 h). (E) WB analysis of APP in WT and APP-KO mouse brain whole-cell lysates. (F) Quantification of MT stability (residual βIII-tubulin levels) in WT or APP-KO mouse hippocampal and cortical neurons (19 DIV). Control, vehicle. (G) EGFP-EB3 analysis of MT dynamics parameters in WT or APP-KO neurons (19 DIV) ± Aβ (200 nM, 1.5 h). Data are shown as means ± SEM. *, $P < 0.05$; **, $P < 0.01$; ***, $P < 0.001$ by two-tailed Student's *t* test based on experiments (B, $n = 3$) or one-way ANOVA followed by Tukey's multiple comparison test based on neurites (C, $n = 36$; D, $n = 9–13$; F, $n = 30$; G, $n = 7–10$). NZ, nocodazole.

found that a dose of SMIFH2 that did not affect MT dynamics nor spine density on its own significantly antagonized spine loss induced by Aβ (Fig. 4, A and B). When analyzed at the morphological level, the rescue was largely caused by an increase in stubby spines (Fig. 4 B). To confirm rescue of short-term synaptotoxicity, we tested the effects of formin inhibition on the deficits in the amplitude of long-lasting duration (maintenance phase) of CA3-CA1 LTP in J20 mice, a line that possesses the Swedish (K670N/M671L) and Indiana (V717F) hAPP mutations (Saganich et al., 2006; Pozueta et al., 2013b). A low dose of formin inhibitor alone did not significantly affect basal synaptic transmission in rat hippocampal cultured neurons (Fig. 4, C and D) or acute hippocampal slices from WT mice (Fig. 4, E and F). The same dose, however, significantly ameliorated the deficits in CA3-CA1 LTP induction in hippocampal slices from J20 mice (Fig. 4, G and H), underscoring a role for formin activity in the acute weakening of synapses associated with memory loss induced by Aβ.

We examined the association of mDia1 to MTs in neurites using conventional confocal microscopy and found that it localized in proximity to both stable and dynamic MTs in axons and dendrites (Fig. 5 A). Higher-resolution confocal microscopy using an Airyscan detector confirmed the association of mDia1 with Glu MTs in axons and both Glu and Tyr MTs in dendrites (Fig. 5, B and C). To examine the role of mDia1 on MT behavior, we silenced mDia1 expression by lentiviral delivery of shRNA in 14-d-in-vitro (DIV) hippocampal neurons for either 4 or 7 d. We found that loss of ≥60% of mDia1 expression after 7 d of infection, but not its closely related formin FHOD1, reduced MT stability and increased the catastrophe frequency of dynamic MTs in untreated neurons (Fig. 5, D–G; and Fig. S4). 1 µM SMIFH2 for 3 h, a time at which this dose of SMIFH2 alone had a significant effect on catastrophe frequency (Fig. S2 E), did not produce additive effects on MT dynamics in mDia1–knocked down neurons, confirming that mDia1 is the primary target of SMIFH2's activity on MTs (Fig. 5 H).

In addition to their effects on MTs, formins are actin nucleators and elongators (Chesarone et al., 2010). The actin functions of mDia1 are involved in the generation of stress fibers (Hotulainen et al., 2009) and in the regulation of phagocytosis (Colucci-Guyon et al., 2005; Brandt et al., 2007; Lewkowicz et al., 2008). To examine the contribution of its actin activity, we generated two actin-null mutants of mDia1 (I845A and K994A) predicted to abrogate mDia1 binding to actin (Xu et al., 2004; Bartolini et al., 2008) and evaluated their ability to restore normal MT catastrophe frequency in mDia1-

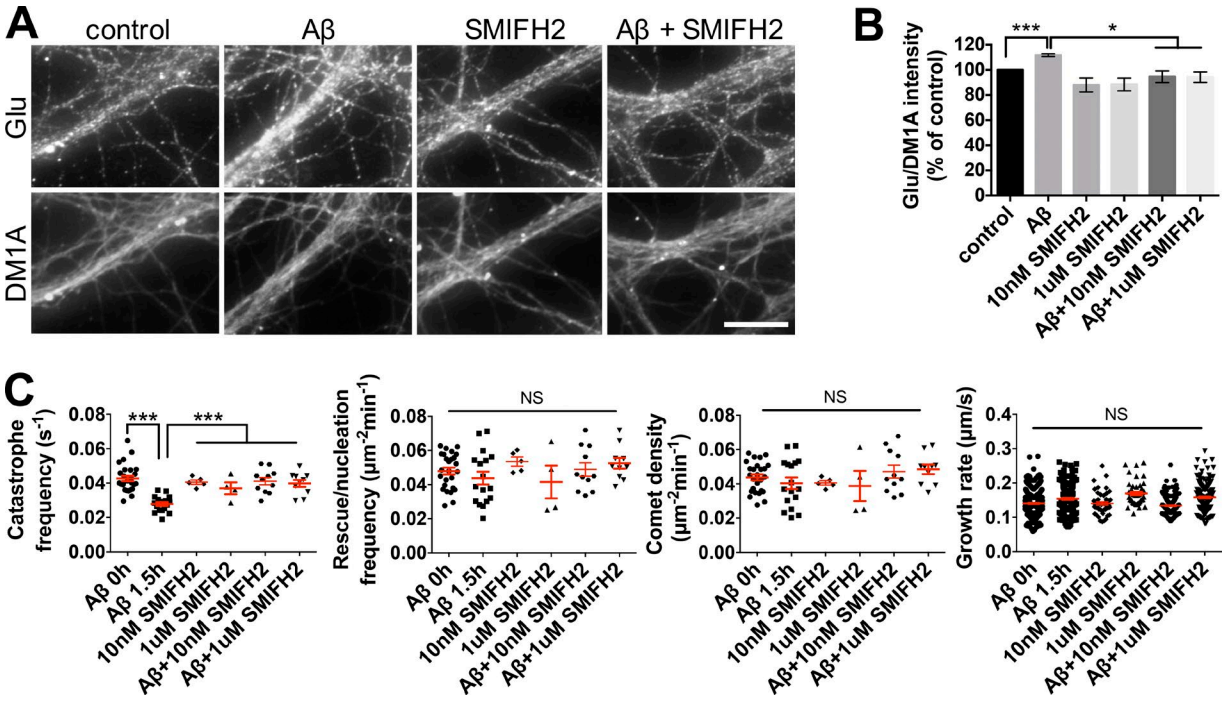

Figure 3. **Formin activity mediates MT stabilization by Aβ.** (A) IF of Glu and total α-tubulin (DM1A) in hippocampal neurons treated with 200 nM Aβ for 2.5 h or with SMIFH2 (1 µM) 30 min before Aβ treatment. Bar, 10 µm. (B) Quantification of Glu/DM1A ratio measured on individual proximal neurites and normalized against vehicle control levels (control) of hippocampal neurons treated as in A. (C) EGFP-EB3 analysis of MT dynamics parameters in hippocampal neurons (18 DIV) treated with Aβ for 1.5 h or with SMIFH2 30 min before Aβ treatment. Data are shown as means ± SEM. *, $P < 0.05$; ***, $P < 0.001$ by one-way ANOVA followed by Dunnett's multiple comparison test based on experiments (B, $n = 3$) or neurites (C, $n = 5–15$).

depleted neurons. Indeed, the increase in catastrophe frequency caused by mDia1 depletion was normalized by either WT or actin-null mDia1, ruling out actin-related functions of mDia1 (Fig. 5 I). Accordingly, a low dose of SMIFH2 that antagonized Aβ-driven changes in MT behavior had negligible effects on Aβ internalization, further ruling out actin-dependent mDia1-mediated phagocytosis (Fig. S2, F–H).

We investigated the result of loss of mDia1 expression on spine number and dendritic morphology and found a significant increase in spine density and dendritic complexity in mDia1-depleted cells (7 d) compared with control levels (Fig. 5, J–L), indicating a role for mDia1 in the post-developmental regulation of structures that are severely affected by Aβ. To test whether mDia1 was an effector of Aβ rather than a permissive factor in the induction of neuronal injury, we examined whether reduction of mDia1 expression (4 d) to levels that would not affect MTs, mitochondria motility, or synaptic density and strength was still sufficient to antagonize Aβ neurotoxicity. Indeed, we found that even partial mDia1 silencing completely suppressed both the decline in MT dynamics and axonal mitochondrial motility caused by Aβ exposure (Fig. 6, A–D). Furthermore, the loss of dendritic spine density induced by Aβ was fully prevented in mDia1-depleted cells compared with control levels (Fig. 6, E and F). Importantly, restoration of the number of synapses was observed with two independent mDia1 shRNAs, and both WT and the actin-binding–deficient K994A mDia1 mutant (Bartolini et al., 2008) expressed in mDia1-silenced cells significantly abrogated the rescue of synapse loss, further ruling out off-target effects and reliance on mDia1-mediated actin functions. Finally, loss of mDia1 expression normalized Aβ-induced perturbations of miniature excitatory postsynaptic currents (mEPSCs) in dissociated hippocampal neurons (Fig. 6 G), demonstrating a role for mDia1 in both pre- and postsynaptic injury caused by Aβ. Collectively, these data strongly position the MT activity of the formin mDia1 in the Aβ cascade that leads to synaptotoxicity, suggesting a primary role for stabilization of dynamic MTs in the onset of synaptic damage.

mDia1 regulates tau phosphorylation through MT stabilization

We investigated whether the mechanism of rescue was intrinsic to regulation of tau phosphorylation by mDia1 through its control of MT stability. MT-destabilizing drugs have been shown to reduce tau phosphorylation at AT8 (202/205/208) and PHF-1 (396/404) phosphoepitopes while increasing Tau-1 (a site that is recognized only when Ser195, 198, 199, and 202 are dephosphorylated; Brion et al., 1994), suggesting that stable MTs may regulate tau-specific kinases and/or phosphatases. Interestingly, incubations with Aβ exert the opposite effects by increasing AT8 and PHF-1, two of the phosphoepitopes associated with NFTs in AD brains, while reducing Tau-1 (Alvarez et al., 1999). We found that robust formin inhibition in young neurons (expressing only the 0N3R tau isoform but high levels of PHF-1, AT8, pT212, and pS262 tau) led to detectable loss of PHF-1 in a time- and dose-dependent fashion (Fig. S5, A and B). Formin inhibition alone further led to loss of AT8, pT212/S214, and pS262 while increasing Tau-1 levels, but it had no effect on pY18, a substrate residue for Fyn kinase (Lee et al., 1998; Ittner et al., 2010), or tau degradation (the same electrophoretic shift in total tau was observed when tau was detected using antibodies directed at either a C- or a N-terminal epitope; Fig. S5, A–F). We chose to focus on pS262 and AT8 for the following reasons: (A) pS262 is an early marker of cytopathology in AD, and its phosphorylation can change tau–MT binding

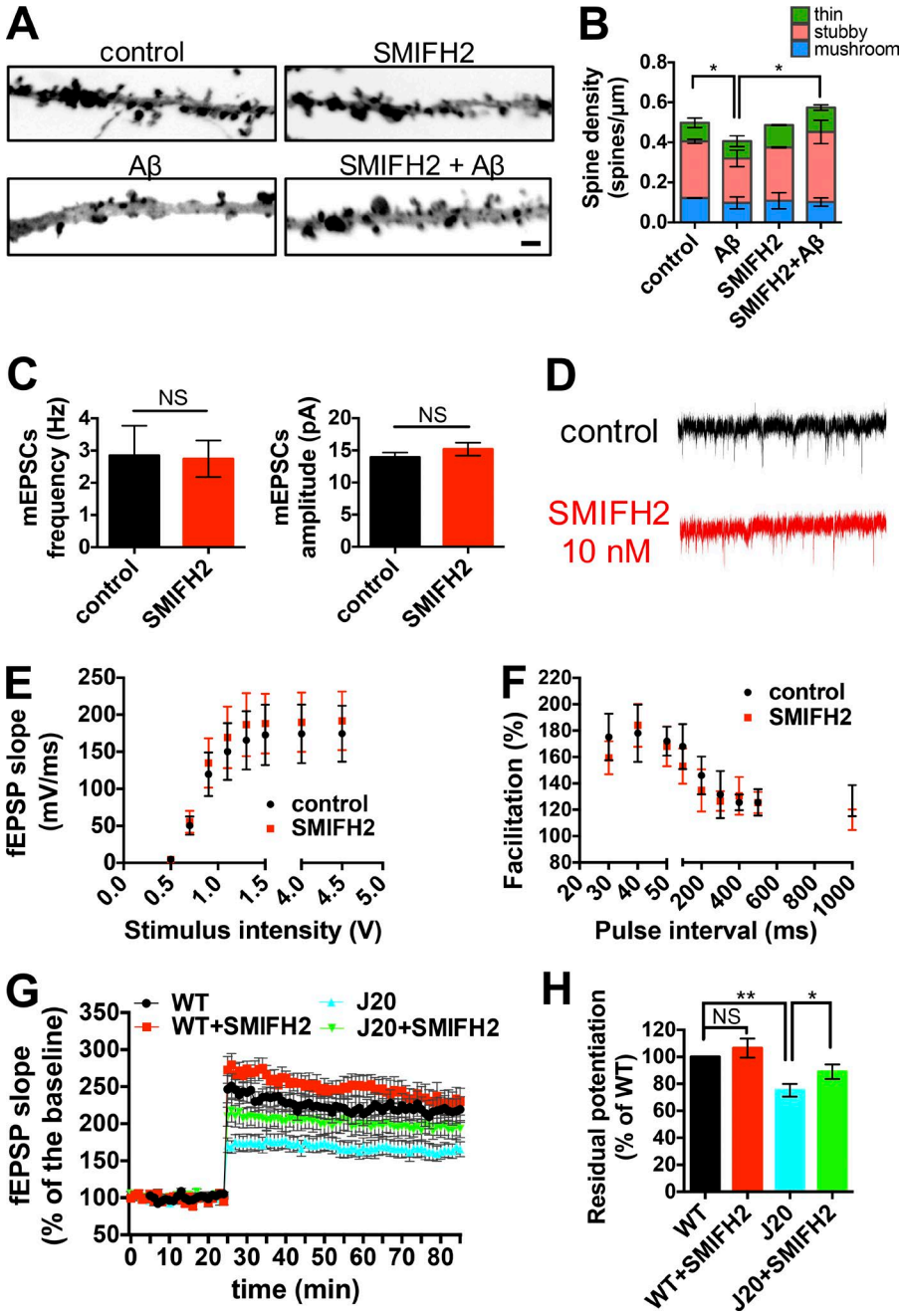

Figure 4. **Formin activity is necessary for synaptotoxicity caused by Aβ.** (A) Representative images of spine density and morphology in primary hippocampal neurons (14 DIV) treated with 200 nM Aβ ± 10 nM SMIFH2 for 24 h. Bar, 2 µm. (B) Quantification of spine density and morphology of neurons treated as in A. (C) Summary bar graphs of the frequency and amplitude of mEPSCs recorded from hippocampal neurons exposed to either vehicle (n = 26) or 10 nM SMIFH2 (n = 36). (D) Sample traces of recordings shown in C. (E and F) Input/output relationship (E; n = 10) and paired-pulse facilitation (F; n = 5) measured in acute hippocampal slices from 10-mo-old WT mice. (G) LTP induced by 3-theta bursts in acute hippocampal slices from 10–12-mo-old WT and J20 mice (n = 7–11). (H) Bar graph representing the mean of the last 15 min of recordings. Data are shown as means ± SEM. *, $P < 0.05$; **, $P < 0.01$ by one-way ANOVA followed by Tukey's multiple comparison test based on neurites (B, $n > 10$), one-tailed Student's t test based on cells (C, n = 26 and 36) or slices (H, n = 7–11).

affinity directly (Biernat et al., 1993; Fischer et al., 2009); (B) AT8 is secondary to pS262 and stains NFTs in AD (Bertrand et al., 2010); (C) both pS262 and AT8 epitopes are induced by Aβ (Zempel et al., 2010). We tested mDia1 regulation of these epitopes and found significant loss of pS262 and AT8 tau in hippocampal neurons silenced of mDia1 expression (Fig. 7, A and B), supporting a physiological role for mDia1 in regulating the phosphorylation of two key residues associated with Aβ pathogenesis. Importantly, loss of tau phosphorylation in mDia1-depleted cells was normalized by restoring MT stability with taxol, reinforcing the model that mDia1 regulation of MT stability is necessary for Aβ-mediated induction of hyperphosphorylated tau. Consistently, acute mDia1 inhibition by a low dose of SMIFH2 had negligible effects on its own but significantly antagonized AT8 tau induction by Aβ (Fig. 7, C and D). Collectively, these data strongly implicate the formin mDia1 as an Aβ effector in the regulation of tau phosphorylation through its control of MT stability.

Acute stabilization of dynamic MTs causes tau hyperphosphorylation and spine loss through tau

We investigated whether inhibition of MT dynamics alone was sufficient to enhance tau hyperphosphorylation and loss of synapses. We used developing neurons (7 DIV) with higher levels of dynamic MTs to biochemically detect low increases in MT stability and found that 10 nM taxol, which inhibits MT dynamics without inducing MT polymerization or bundling (Derry et al., 1995), promoted a detectable increase in tubulin PTMs and both AT8 and pS262 tau within 3 h (Fig. 8, A–C). Taxol, which does not influence MT interaction with tau (Kadavath et al., 2015), further resulted in repartition of endogenous tau

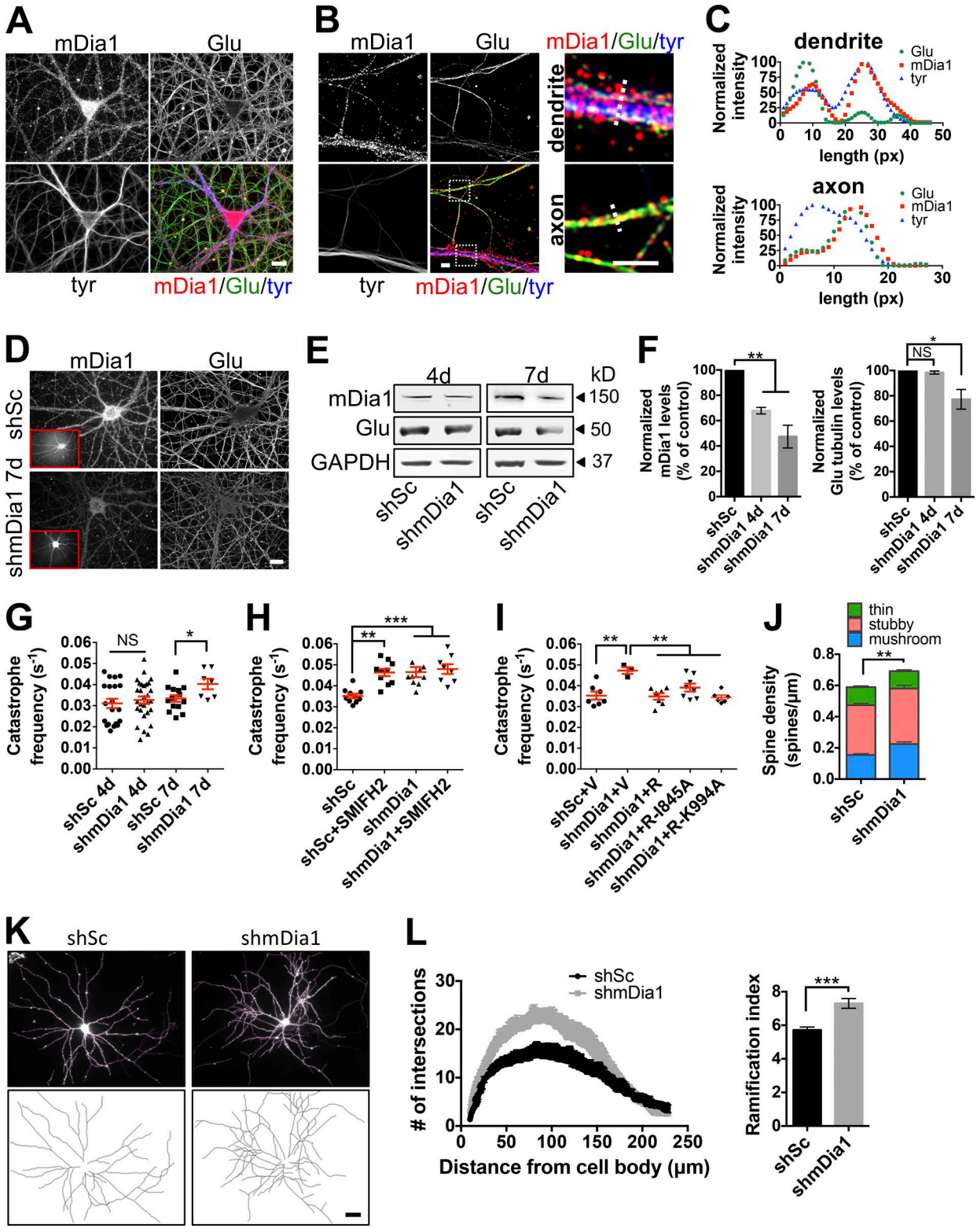

Figure 5. **mDia1 regulates MT stability, MT dynamics, and dendrite complexity in neurons.** (A) IF staining of mDia1, Glu, and tyrosinated (Tyr) tubulin in hippocampal neurons (21 DIV). Bar, 20 µm. (B) Higher-resolution imaging of samples as in A. White dotted lines show cross-section drawings in insets marked by white dotted boxes. Bar, 2 µm. (C) Linescan measurements of IF intensity from cross-sections shown as in B. Fluorescent intensities are expressed as percentages of the maximum intensity for each indicated channel. (D) IF staining of mDia1 and Glu tubulin in hippocampal neurons (21 DIV) treated with scrambled control (shSc) or shRNA against mDia1 (shmDia1) lentiviruses for 7 d. Inset images show GFP signals from lentiviral infection. Bar, 20 µm. (E) WB analysis of mDia1 and Glu tubulin levels in hippocampal neurons (18 or 21 DIV) treated with shSc or shmDia1 lentiviruses for 4 or 7 d. (F) Quantification of mDia1 and Glu tubulin levels normalized against GAPDH levels in 4- or 7-d mDia1-silenced neurons. (G–I) EGFP-EB3 analysis of MT catastrophe frequency in hippocampal neurons infected with shSc or shmDia1 lentiviruses for 4 or 7 d (18 or 21 DIV; G), infected with lentiviruses for 7 d ± 1 µM SMIFH2 for 3 h (21 DIV; H), or infected with lentiviruses (14 DIV) and transfected (19 DIV) with pmCherry-C1 vector control (V), WT mDia1 shRNA

from a MT pellet to a soluble fraction (Fig. 8 D). To visualize whether this also occurred with the longest tau variant, we imaged the dynamics of EGFP-tau2N4R together with RFP-tubulin in NIH3T3 cells and found that taxol induced rapid tau dissociation from MTs with a negligible loss in the MT label caused by photobleaching (Fig. 8, E and F). We hypothesized that tau dissociation from MTs induced by taxol resulted from MT-dependent induction of tau phosphorylation at S262, a crucial residue directly involved in tau–MT binding and negatively regulated by phosphorylation (Fischer et al., 2009). Indeed, an S262A phospho-null version of EGFP-tau2N4R completely lost its ability to dissociate from MTs upon taxol exposure (Fig. 8, E and F), strongly indicating a role for stabilization of dynamic MTs in the regulation of one or more S262 tau-specific kinases and/or phosphatases.

We have observed that even transient inhibition of dynamic MTs by Aβ may contribute to chronic neuronal injury. To explore whether acute stabilization of dynamic MTs alone had long-term effects on synaptic density, we measured the damage inflicted on spines by acute exposures to a low dose of taxol. Indeed, acute taxol exposure reduced dendritic spine density both at short (3 h) and long (3 h followed by 21 h washout) time points to levels comparable to chronic (24 h) incubations with Aβ (Fig. 8, G and H). To interrogate the role of tau in the induction of synaptic damage by inhibition of MT dynamics, we compared dendritic spine density between WT and tau-KO neurons upon either Aβ or acute taxol exposure. Strikingly, loss of dendritic spines induced by either acute taxol or Aβ exposure was significantly antagonized in tau-KO neurons, which appeared to be only weakly affected compared with vehicle control (Fig. 8, I and J).

Collectively, these data strongly suggest that even transient stabilization of dynamic MTs is sufficient to induce long-term loss of synapses and argue for a primary role of stabilization of dynamic MTs in the damage inflicted by Aβ on synapses through induction of hyperphosphorylated tau.

Discussion

We found that Aβ induces acute stabilization of dynamic MTs through mDia1-mediated inhibition of MT catastrophe frequency, an activity contributing to tau hyperphosphorylation and synaptotoxicity (Fig. 9). No significant effect of Aβ was observed on growth rates or comet density, ruling out MT sliding or selective depolymerization of the labile region of neuronal MTs by Aβ (Baas et al., 2016; Matamoros and Baas, 2016).

Our observations are particularly interesting after the recent discovery that the early phase of memory formation is associated with a decrease in detyrosinated tubulin associated with MT stability and that learning-induced MT destabilization is crucial for long-term memory and synaptic plasticity (Uchida et al., 2014; Uchida and Shumyatsky, 2015). Consistently, inhibition of MT dynamics was recently reported in neurons from Kif21b-KO mice that exhibit learning and memory disabilities (Muhia et al., 2016). Thus, it is tempting to speculate that Aβ-mediated loss of cognitive function in AD could be contributed by progressive Aβ-mediated inhibition of MT dynamics at early stages of memory formation when MTs need to be highly dynamic to induce long-lasting changes in synaptic function.

We observed that Aβ leads to accumulation of tubulin detyrosination and acetylation while promoting acute inhibition of MT dynamics. Indeed, induction of tubulin detyrosination itself is of particular interest. Tubulin detyrosination offers protection from the depolymerizing activity of kinesin-13–type motor proteins such as KIF2 or mitotic centromere-associated kinesin (Peris et al., 2009; Sirajuddin et al., 2014) and negatively regulates the binding of +TIPs with CAP-Gly domains such as CLIP170 or p150/glued (Honnappa et al., 2006; Peris et al., 2006; Bieling et al., 2008; McKenney et al., 2016; Nirschl et al., 2016). In contrast, the molecular motors kinesin-1 and kinesin-2 move preferentially on Glu MTs in vitro and in cells (Kreitzer et al., 1999; Konishi and Setou, 2009; Kaul et al., 2014; Sirajuddin et al., 2014). In neurons, these functions are all predicted to regulate the trafficking of MT-dependent organelle cargos, neurite branching, and synapse maintenance. Thus, the damage induced by up-regulating Glu-tubulin in adult neurons may contribute to the dysfunction of multiple neuronal pathways. Further investigation is required to test this model.

We find that APP is required for stabilization of dynamic MTs by Aβ. APP has been classically implicated in synaptotoxicity as it is directly related to the production of Aβ. However, compelling evidence has also recently shown that APP signaling is critical for the toxic effect of extracellular oligomeric Aβ on synaptic activity, memory, and LTP (Fogel et al., 2014; Puzzo et al., 2017), suggesting that dynamic MT stabilization by Aβ, also dependent on APP, contributes to synaptotoxicity downstream of APP signaling. To our knowledge, this is the first study of APP as a MT-regulating factor. Further studies are required to dissect the mechanisms by which APP may control Rho activation either directly or through integrin function.

We provide compelling evidence that inhibition and silencing of the formin mDia1 suppressed the Aβ-mediated MT activity in primary neurons and corrected defects in axonal transport and synaptotoxicity induced by Aβ. The involvement of a formin in the induction of Aβ-mediated synaptotoxicity is novel but consistent with prior observations. Formin activity has been implicated in the generation of dynamic cytoskeletal structures required for dendritic spines, axonal actin trails, and actin-mediated vesicle fusion and endocytosis at nerve terminals (Salomon et al., 2008; Hotulainen et al., 2009; Law et al., 2014; Ganguly et al., 2015; Deguchi et al., 2016; Soykan et al., 2017). In the case of mDia1, however, we provide multiple lines of evidence indicating that the actin-independent MT activity of this formin contributes to neuronal injury caused by Aβ: (A) two actin binding–deficient mutants of mDia1 normalized MT dynamics defects in mDia1-depleted neurons at comparable levels to WT mDia1; (B) loss of actin binding did not

resistant (R), I845A actin-null mDia1 shRNA resistant (R-I845A), or K994A actin-null mDia1 shRNA resistant (R-K994A; 21 DIV; I). Data are analyzed from 41–253 comets for each group. (J) Quantifications of spine density and morphology in hippocampal neurons (21 DIV) infected with shSc or shmDia1 lentiviruses for 7 d. (K) Representative images and schematics of hippocampal neurons (21 DIV) infected with shSc or shmDia1 lentiviruses for 7 d. Bar, 50 µm. (L) Number of intersections from the cell body and ramification index by Sholl analysis in neurons infected as in K. Data are shown as means ± SEM. *, P < 0.05; **, P < 0.01; ***, P < 0.001 by two-tailed Student's *t* test based on experiments (F, *n* = 3), neurites (J, *n* = 22), or cells (L, *n* = 15), or one-way ANOVA followed by Tukey's multiple comparison test based on neurites (G–I, *n* = 3–29).

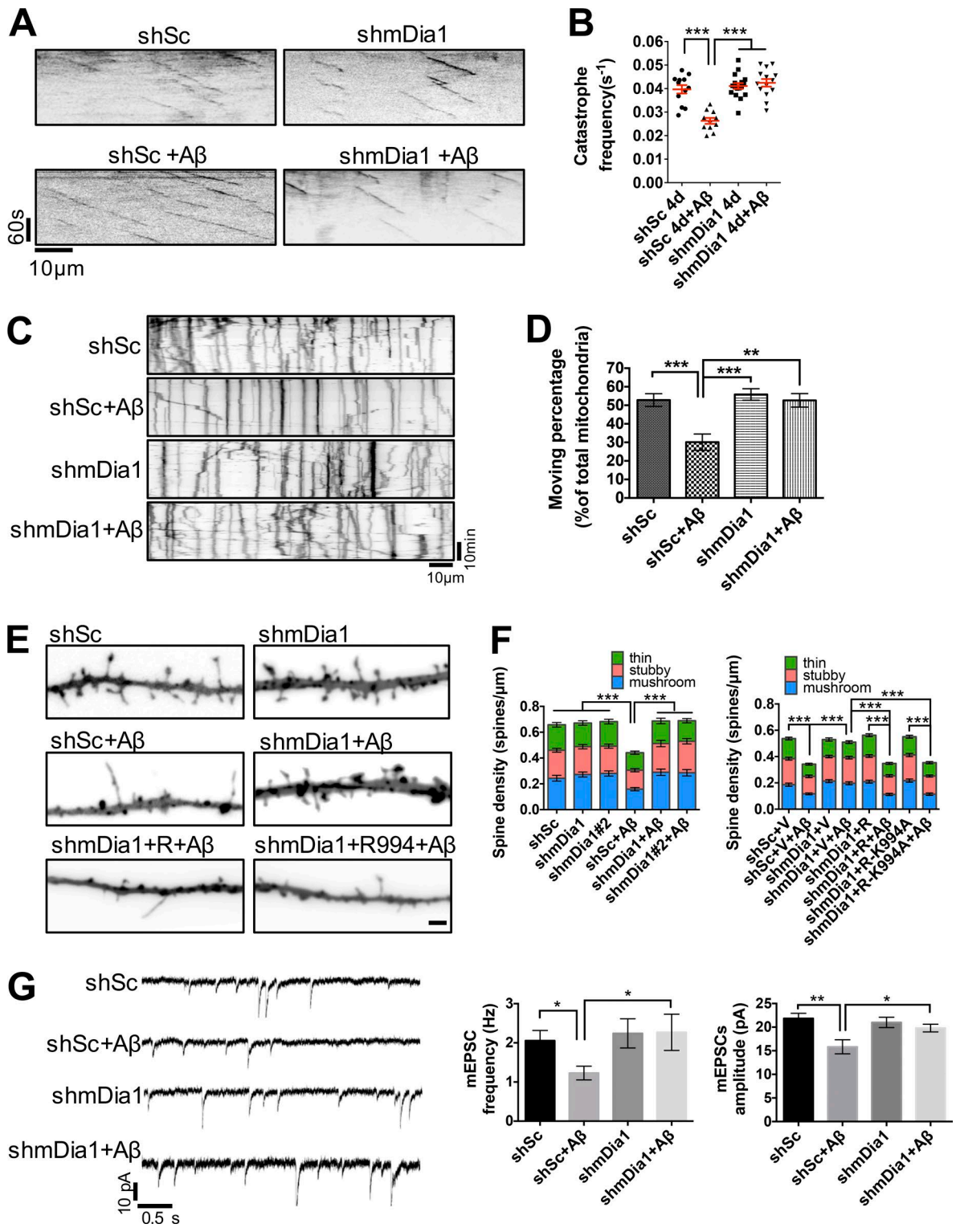

Figure 6. **mDia1 mediates inhibition of MT dynamics, axonal transport defect, and synaptotoxicity induced by Aβ.** (A) Representative kymographs of hippocampal neurons (18 DIV) infected with shSc or shmDia1 lentiviruses for 4 d ± Aβ (200 nM, 1.5 h). (B) MT catastrophe frequency in hippocampal neurons treated as in A. Data are analyzed from 114–196 comets for each group. (C) Representative kymographs of mitochondrial motility in hippocampal neurons (10 DIV) infected with shSc or shmDia1 lentiviruses for 4 d and transfected with mito-DsRed2. Videos (10 s/frame for 30 min) were taken before and after 6 h treatment with 200 nM Aβ. (D) Quantification of the percentage of moving mitochondria. (E and F) Spine density and morphology in hippocampal neurons (18 DIV) infected with shSc or two different shRNAs against mDia1 for 4 d and treated with Aβ for 24 h or infected with lentiviruses (14 DIV) and transfected (17 DIV) with pmCherry-C1 vector control (V), shmDia1-resistant mutant (R), and shmDia1 resistant + K994A actin mutant (R-K994A) and then treated with Aβ for 24 h. Bar, 2 μm. (G) Representative trace plots and summary bar graphs of frequency and amplitude of mEPSC recordings from cultured hippocampal neurons (18 DIV) infected with shSc or shmDia1 lentiviruses and exposed to either vehicle or 1 μM Aβ for 6 h. Data are shown as means ± SEM. *, $P < 0.05$; **, $P < 0.01$; ***, $P < 0.001$ by one-way ANOVA followed by Tukey's multiple comparison test based on neurites (B, $n = 11–17$; D, $n = 7–11$; F, $n = 37–60$) or two-tailed Student's t test based on cells (G, $n = 19–22$).

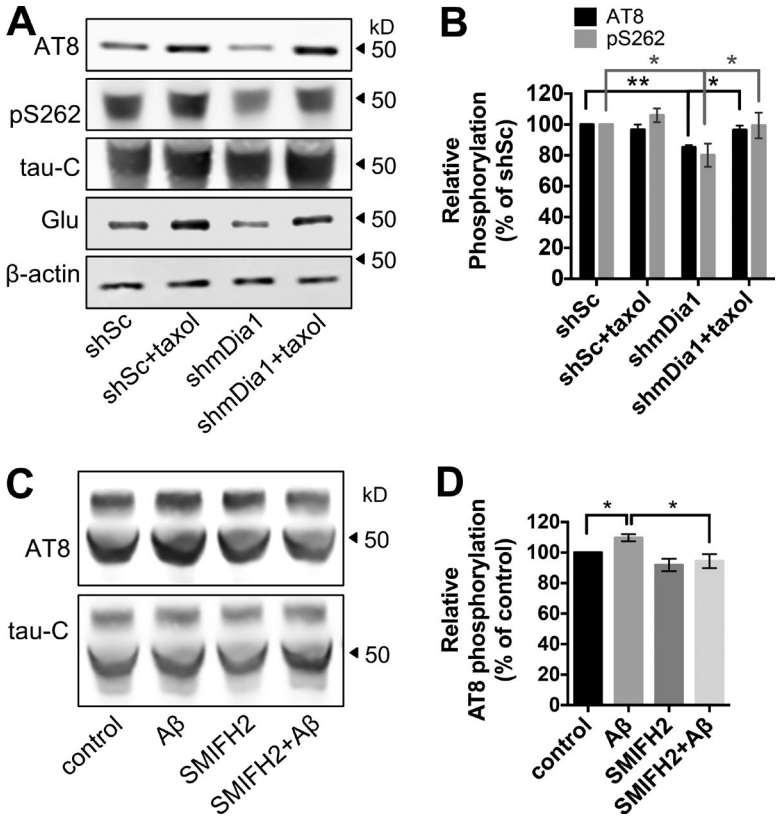

Figure 7. **mDia1 regulates tau phosphorylation through MT stability.** (A) WB analysis of phosphorylated (AT8 and pS262) and total (tau-C) tau levels in hippocampal neurons (21 DIV) silenced for mDia1 expression (7 d) ± taxol (10 nM) for 3 h. (B) Quantification of normalized AT8 and pS262 levels in neurons treated as in A. (C) WB analysis of SMIFH2 (1 µM) inhibition on hyperphosphorylated tau (AT8) induced by Aβ (200 nM, 6 h) in hippocampal neurons (18 DIV). (D) Quantification of normalized AT8 levels in neurons treated as in C. Control, vehicle. Data are shown as means ± SEM. *, $P < 0.05$; **, $P < 0.01$ by two-tailed Student's *t* test ($n = 3–5$).

prevent mDia1 from mediating neuronal injury induced by Aβ; (C) normalization of MT stability reinstated normal levels of tau phosphorylation in neurons silenced of mDia1 expression. We observed that mDia1 regulates MT stability and catastrophe frequencies in untreated neurons and downstream of Aβ. Thus, it appears that whereas in NIH3T3 cells, mDia1 stabilizes MTs by hindering plus end growth and shrinkage rates (Bartolini et al., 2016), in neurons, it inhibits MT dynamics by limiting their catastrophe frequencies. Although we cannot yet fully explain this difference, we speculate that it may reflect an intrinsic divergence in the mechanisms that lead to the stabilization of densely packed noncentrosomal MTs present in neurons as opposed to radial MT arrays making their way through a thick actin network observed in nonneuronal cells.

We found that loss of mDia1 expression antagonized inhibition of pre- and postsynaptic function caused by Aβ in cultured hippocampal neurons. A role for the fly orthologue of mDia1 in presynaptic growth and maintenance has been highlighted in the neuromuscular junction, where it regulates the behavior of dynamic pioneer MTs at the presynaptic terminal (Pawson et al., 2008). Additional studies are necessary to assess a role for mDia1 and perhaps other formins in the regulation of dynamic MTs in mammalian presynaptic boutons and/or postsynaptic sites in health and disease. Notably, we found that acute mDia1 inhibition also ameliorated LTP deficits in J20 mice at an age at which LTP is strongly impaired and plaques are abundant. That this process occurs long after the appearance of amyloid plaques suggests that formin inhibition may normalize synaptic alterations crucial for learning and memory even after disease diagnosis, paving the way to development of therapeutic strategies aimed at modulating formin function.

We have shown that reestablishing MT stability was sufficient to restore tau phosphorylation in mDia1-silenced neurons. Furthermore, acute inhibition of MT dynamics alone promoted tau dissociation from MTs through phosphorylation of S262 on tau, a key residue for the binding of tau to MTs. These observations break ground for the analysis of MT end-binding proteins and tubulin PTMs in the regulation of tau phosphorylation as well as tau-dependent synaptic pruning through modulation of tau-specific kinase and/or phosphatase activities. Indeed, multiple kinases and phosphatases are regulated by their association with MTs or MAPs, strongly indicating MTs as signaling platforms for the transduction and coordination of cellular pathways in response to cytoskeletal changes. As a range of stimuli may produce different changes in MT behavior, +TIP binding, or accumulation of tubulin PTMs, it will be of considerable interest to further explore the relative contributions of these mechanisms for regulating kinase or phosphatase activities in health and a wider spectrum of neurodegenerative diseases.

We found that acute stabilization of dynamic MTs is sufficient to induce spine loss comparable to chronic Aβ exposure. MT integrity has been implicated in dendritic spine density and morphology, synaptic plasticity, and memory formation (Fanara et al., 2010; Zempel et al., 2010; Atarod et al., 2015), but the precise role of MT stability and dynamics in synaptotoxicity is still controversial. Despite clear differences between Aβ- and taxol-specific MT activities, our data are consistent with findings that nocodazole at doses that dampen MT dynamics without inducing massive MT depolymerization leads to loss of spines and defects in synaptic plasticity (Jaworski et al., 2009; Fanara et al., 2010; Penazzi et al., 2016). We acknowledge that taxol and analogous drugs were found to ameliorate Aβ-induced synaptotoxicity in hippocampal slices and animal models of neurodegenerative disease (Brunden et al., 2010; Fanara et al., 2010; Penazzi et al., 2016; Ballatore et al., 2017). We note, however, that it is difficult to assess the accurate neuronal

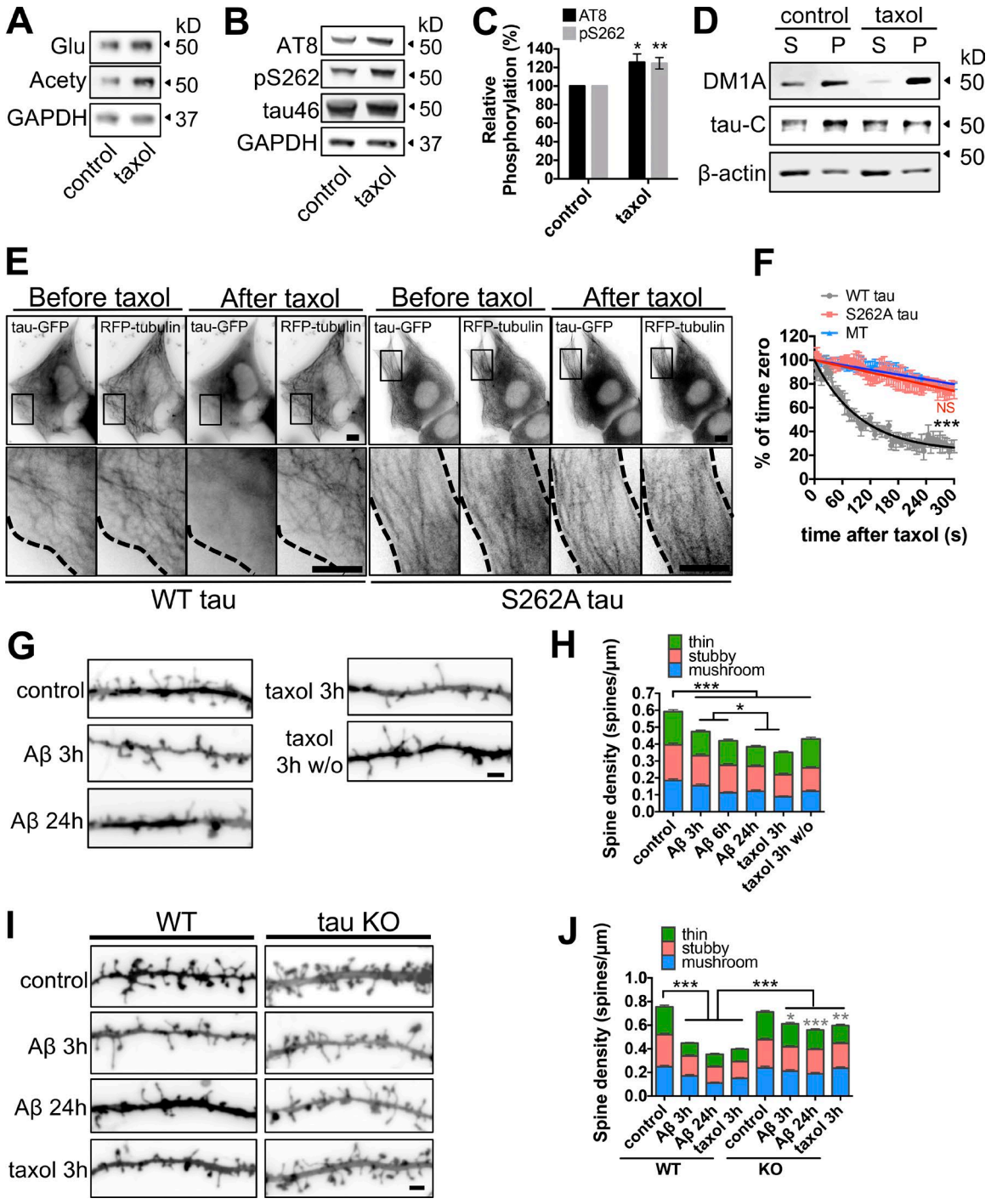

Figure 8. **Inhibition of MT dynamics causes tau hyperphosphorylation and spine loss though tau.** (A and B) WB analysis of Glu and acetylated (Acety) tubulin (A) as well as phosphorylated (AT8 and pS262) and total (tau-46) tau levels (B) in hippocampal neurons (7 DIV) incubated with 10 nM taxol for 3 h. (C) Quantification of normalized AT8 and pS262 against control levels in taxol-treated neurons. (D) WB analysis of total tau (tau-C) and tubulin (DM1A) levels in cortical neurons (7 DIV) treated with 10 nM taxol for 3 h. Aliquots of soluble (S) and MT pellet (P) fractions are shown. (E) Representative images from time-lapse recordings of NIH3T3 cells cotransfected with human 2N4R WT or S262A tau-GFP and RFP-tubulin before and 10 min after 10 nM taxol. Dashed lines indicate cell peripheries. Bar, 20 µm. (F) Quantification of background-subtracted MT-bound WT tau, S262A tau, and MT intensity after taxol treatment. (G and H) Representative images (G) and quantification (H) of spine density and morphology of hippocampal neurons (21 DIV) treated with vehicle control, Aβ, or taxol for the indicated times ± washout (w/o). (I and J) Representative images (I) and quantification (J) of spine density and morphology of hippocampal neurons (21 DIV) from WT and tau-KO mice treated with vehicle control, Aβ, or taxol for the indicated times. Bars, 2 µm. Gray asterisks in J compare Aβ- or taxol-treated KO neurons to KO control neurons. Data are shown as means ± SEM. *, $P < 0.5$; **, $P < 0.01$; ***, $P < 0.001$ by two-tailed Student's *t* test based on experiments (C, $n = 3$) or cells (F, $n = 6$) comparing to control (C) or MT intensity (F) or by one-way ANOVA followed by Tukey's multiple comparison test based on neurites (H, $n = 124–151$; J, $n = 42–70$).

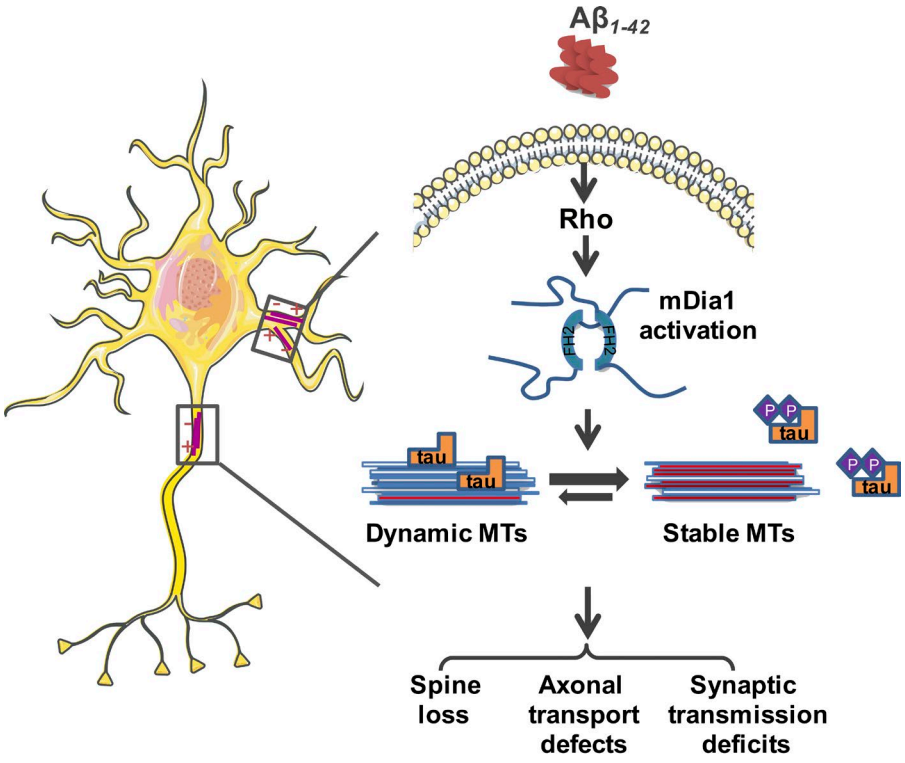

Figure 9. **Working model for mDia1-mediated stabilization of dynamic MTs in Aβ-induced synaptotoxicity.** Aβ induces the formation of "toxic" subsets of stabilized MTs through Rho signaling and mDia1 activation in neurons. Stabilized MTs cause a cellular stress response that leads to tau dissociation and hyperphosphorylation in the attempt to restore normal levels of dynamic and unmodified MTs. Induction of these neurotoxic pathways results in spine loss, axonal transport, and synaptic transmission deficits.

concentration of the drug from the in vivo studies, and the doses used in the ex vivo experiments are 10-fold lower than the dose used in our in vitro studies. We believe that this difference may limit the interpretation of these studies, as no information is available on the cellular effects of taxol on MTs or tubulin at subnanomolar concentrations.

We found that spine loss caused by either Aβ or taxol was significantly mitigated in tau-KO neurons, suggesting a crucial role of tau-dependent synaptotoxicity downstream of the loss of a dynamic MT cytoskeleton. Our results are consistent with several prior in vitro and in vivo studies in which Aβ synaptotoxicity depended on endogenous tau and was exacerbated by the expression of human tau (Rapoport et al., 2002; Roberson et al., 2007; Ittner et al., 2010; Vossel et al., 2010; Jin et al., 2011; Mairet-Coello et al., 2013; Zempel et al., 2013). Importantly, we found that inhibition of MT dynamics is sufficient to dissociate tau from MTs upon S262 tau phosphorylation. Further analyses are required to establish the role of tau dissociation and phosphorylation in the synaptic damage inflicted by inhibition of MT dynamics and the mechanisms by which MT-dependent tau hyperphosphorylation is achieved.

In conclusion, our studies provide compelling evidence that acute MT stabilization of dynamic MTs rather than global MT destabilization may initiate Aβ synaptotoxicity. This paradigm-shifting model does not reject loss of MT integrity as a major pathological feature of chronic Aβ exposure but rather provides a unifying theory for the induction of tau hyperphosphorylation and neuronal injury by defining primary and secondary consequences on MT stability caused by Aβ. In our pathogenesis model, promotion of hyperphosphorylated tau and MT disassembly would result from a cellular response to Aβ-mediated induction of toxic subsets of less dynamic and modified MTs, which may have occurred at early stages of the disease. Consistent with this interpretation, tubulin PTMs associated with nondynamic MTs have been shown to regulate MT severing (Lacroix et al., 2010; Leo et al., 2015), and loss of tau binding may further sensitize stable MTs to severing enzymes (Qiang et al., 2006; Sudo and Baas, 2010). Hyperphosphorylated tau may have additional gain-of-function roles such as toxic effects by tau tangles themselves and in the targeting of severing enzymes to dendritic MTs (Zempel et al., 2013).

Regardless of whether injury to the dynamic MT cytoskeleton plays a primary role within a larger spectrum of neurodegenerative diseases, a great deal of work is undoubtedly required to investigate the neuronal pathways by which MT dynamics and tubulin PTMs can be altered by neurotoxic stimuli and the mechanisms by which these MT changes lead to neuronal damage independently and through tau.

Materials and methods

Animals

All protocols and procedures were approved by the Committee on the Ethics of Animal Experiments of Columbia University and according to Guide for the Care and Use of Laboratory Animals distributed by the National Institutes of Health. E18 pregnant Sprague Dawley rats were purchased from Charles River Laboratories. Mouse models used in this study included: tau-KO (E15–16 for culture; parental line was a gift from F. Polleux, Columbia University, New York, NY; Dawson et al., 2001), J20 (10 mo for acute hippocampal slices; The Jackson Laboratory), and APP-KO mice (E15–16 for culture; parental line was a gift from L. D'Adamio, Albert Einstein College of Medicine, New York, NY; Zheng et al., 1995) under the C57BL/6 background.

Reagents and antibodies

All chemicals were obtained from Sigma-Aldrich unless otherwise noted. Primary antibodies used for Western blot (WB) or immunofluorescence (IF) analysis were: mouse anti-$A\beta_{17–24}$ (1:1,000 WB; 4G8; MAB1561; EMD Millipore), rabbit antidetyrosinated tubulin (1:50,000

WB; 1:500 IF; SG; Gundersen et al., 1984), mouse anti–α-tubulin (1:100 IF; DM1A; T9026; Sigma-Aldrich), mouse antiacetylated tubulin (1:50,000 WB; 1:100 IF; 6-11-B1; T7451; Sigma-Aldrich), mouse anti–βIII-tubulin (1:1,000 IF; AB7751; Abcam), mouse anti-GAP DH (1:5,000 WB; AM4300; Ambion), rabbit anti-GAPDH (1:5,000 WB; sc-25778; Santa Cruz Biotechnology, Inc.), mouse anti–β-actin (1:30,000 WB; MAB1501; EMD Millipore), mouse anti-APP (1:1,000 WB; 22c11; MAB348; EMD Millipore), mouse anti-mDia1 (1:500 WB; 610849; BD), rabbit anti-MAP2 (1:400 IF; AB32454; Abcam), rabbit anti-FHOD1 (1:500 WB; sc-99209; Santa Cruz Biotechnology, Inc.), rabbit anti–lamin B1 (1:1,000 WB; sc-56146; Santa Cruz Biotechnology, Inc.), rabbit anti-pSer262 (1:1,000 WB; 44750G; Invitrogen), mouse anti-AT8 (1:1,000 WB; MN1020; Invitrogen), rabbit anti-T212 (1:1,000 WB; AB4842; Abcam), mouse anti–PHF-1 (1:1,000 WB; provided by P. Davies, Albert Einstein College of Medicine, New York, NY), rabbit anti–tau-C (1:1,000 WB; SAB4501823; Sigma-Aldrich), mouse anti-tau46 (1:2,000 WB; sc-32274; Santa Cruz Biotechnology, Inc.), and mouse anti–tau-N (1:500; 3H6.H7; MMS-5065; BioLegend). For WB analysis, secondary antibodies were conjugated to IR680 or IR800 (Rockland Immunochemicals) for multiple infrared detection. For IF analysis, primary antibody incubation was followed by use of the appropriate Alexa Fluor fluorescent dye–conjugated secondary antibodies (Jackson ImmunoResearch Laboratories, Inc.).

Aβ oligomers preparation

Oligomer-enriched preparations of Aβ were obtained according to previously published methods (Stine et al., 2003). Lyophilized Aβ (rPeptide) was equilibrated to room temperature for 30 min to avoid condensation upon opening the vial. The lyophilized peptide was resuspended in 1,1,1,3,3,3-hexafluoro-2-propanol to a concentration of 1 mM for another 2 h at room temperature and then aliquoted into low protein–binding Eppendorf tubes. Monomeric Aβ aliquots were dried under vacuum in a SpeedVac and stored at −80°C. To prepare oligomer-enriched preparations, the aliquots were resuspended in anhydrous DMSO to 5 mM followed by vortexing and 10 min sonication. The resuspended peptide was diluted to 100 µM in ice-cold Ham's F-12 medium, immediately vortexed for 30 s, and then incubated at 4°C for 24 h before use. Total Aβ concentration was measured by BCA assay after oligomerization, and 200 nM of oligomeric Aβ was used in all experiments unless otherwise noted. Scrambled Aβ control (rPeptide) was prepared using same protocol mentioned earlier in this section. TAMRA Aβ (Anaspec) was prepared according to the manufacture's protocol and oligomerized at 4°C for 24 h before use at 200 nM.

Cell cultures and primary hippocampal neuronal cultures

NIH3T3 cells were grown in DMEM and 10% calf serum as previously described (Pianu et al., 2014). Primary hippocampal neuronal cultures were prepared as previously described (Liu et al., 2014). In brief, hippocampi were dissected from E18 rat or E15.5 mouse embryos, and neurons were plated on 100 µg/ml poly-D-lysine–coated 12-well plates at the density of 3×10^5 cells/well for biochemistry assays, 5×10^4 cells/dish for live imaging in the chamber of 35-mm MatTek dishes, 3×10^4 cells/coverslip on 15-mm coverslips for whole-cell patch clamp, or 4×10^4 cells/coverslip on 18-mm coverslips for IF. Primary neurons were maintained in Neurobasal medium (Invitrogen) with the supplement of 2% B-27 (Invitrogen) and 0.5 mM glutamine (Invitrogen), and one third of medium was changed every 3–4 d up to 4 wk in culture.

Lentiviral shRNA silencing

Production of lentiviral particles was conducted using the second generation packaging system as previously described (Liu et al., 2014). In brief, HEK293T cells were cotransfected with lentiviral shRNA constructs and the packaging vectors psPAX2 and pMD2.G (Addgene) using calcium phosphate. 48 and 72 h after transfection, the virus was collected, and the lentiviral particles were concentrated, aliquoted, and stored at −80°C. Two mDia1 shRNA sequences were generated onto pLVT HM vector. mDia1 shRNA 1 was 5′-CGCGTGCGACGGCGGCAA ACATAATTCAAGAGATTATGTTTGCCGCCGTCGCTTTTTTA-3′, and mDia1 shRNA 2 was 5′-CGCGTGCTGGTCAGAGCCATGGAT TTCAAGAGAATCCATGGCTCTGACCAGCTTTTTTA-3′. mDia1 shRNA 1 was used in all knockdown and rescue experiments unless otherwise noted. FHOD1 shRNA sequence with the sequence 5′-CGC GTAGGAGCCGAAGATCACTAGAAGTTCAAGAGACTTCTAGTG ATCTTCGGCTCCTTTTTTTA-3′ was generated onto pLVTHM vector. A scrambled shRNA (pLVTHM-scr) with the oligonucleotide DNA sequence 5′-CGCGTGGCAAATCTTCTAGTCTATTTCAAG AGAATAGACTAGAAGATTTGCCTTTTTTA-3′ was used as control. Lentiviral constructs to knock down tau were purchased from Sigma-Aldrich (TRCN0000091298) with the DNA sequence 5′-CCGGAC AGGAAATGACGAGAAGAAACTCGAGTTTCTTCTCGTCATTTC CTGTTTTTTG-3′ onto a pLKO.1 lentivector. The pLKO.1 vector with a noncoding sequence was used as control.

Plasmid mutagenesis

mDia1 shRNA 1 resistant (R), I845A, and K994A point mutants were generated on pmCherry-C1-mDia1 using the QuikChange Site-Directed Mutagenesis kit (Agilent Technologies) according to the manufacturer's protocol and using the following synthetic sense oligonucleotide primers: 5′-CCTGCGACGGGCGGCGATGGAGGAAAA CATAAGAAATTTACT-3′ (R), 5′-GACAGCGCAGAATCTCTCAGC CTTTTTGGGTTCATTCCGC-3′ (I845A), and 5′-TTGTAAGCTTCG AGACACCGCGTCTGCAGATCAGAAGATG-3′ (K994A). Human 2N4R S262A mutant tau was generated on human EGFP-tau2N4R tau using the QuikChange Site-Directed Mutagenesis kit according to the manufacturer's protocol and using the synthetic sense oligonucleotide primer 5′-TTCAGGTTCTCAGTGGCGCCGATCTTGGACTTG-3′. All constructs were verified by sequencing, and the cDNAs were purified with HiPure Plasmid Maxiprep kits (Invitrogen).

WB analyses

Cells were lysed in Laemmli sample buffer and boiled at 96°C for 5 min. Cell lysates were sonicated by probe sonicator to sheer cellular debris and genomic DNA. To detect tubulins, lysates were diluted 1:10 in sample buffer. Proteins were separated by 10% Bis-Tris gel (Invitrogen) and transferred to nitrocellulose membrane. After blocking in 5% milk/TBS or BSA/TBS, membranes were incubated with primary antibodies at 4°C overnight and 1 h with secondary antibodies. Image acquisition was performed with an Odyssey imaging system (LI-COR Biosciences) and analyzed with Odyssey software.

IF microscopy and analyses

In most immunostaining experiments, cells were fixed in methanol at −20°C for 10 min and rehydrated in TBS, pH 7.4. Cells were stained by double-indirect IF using specific primary antibodies for 30 min followed by secondary antibodies for another 30 min. Mounted samples were observed by epifluorescence microscopy (TE2000-U; Nikon) using a 60× Plan Apochromat objective (1.45 NA). Images were collected with an Orca IIER camera (Hamamatsu) and a Metamorph imaging workstation (Molecular Devices). For MTs and mDia1 immunostainings, cells were fixed in 3.7% PFA, 0.25% glutaraldehyde, 3.7% sucrose, and 0.1% Triton X-100 for 15 min and quenched in 1 mg/ml sodium borohydride/PBS. Cells were then washed in PBS, blocked in 2% FBS, 2% BSA, and 0.2% fish gelatin in PBS for 1 h and then stained with primary antibodies for 2 h followed by secondary antibodies for

another 1 h. Mounted samples were observed by an IX83 microscope (Olympus) with widefield and disk-scanning unit spinning-disk imaging. The microscope was equipped with an IX3-RFA Straight illuminator, a 60× Plan Apochromat oil objective (1.3 NA), and an ORCA R2 Deep-Cooled charge-coupled device camera (Hamamatsu) and was controlled by Metamorph imaging software. Higher-resolution imaging was performed with an LSM 800 confocal microscope (ZEISS) equipped with Airyscan module using a 63× objective (Plan Apochromat, 1.4 NA). Images were obtained and processed using Zen Blue 2.1 software (ZEISS). Dendrites and axons are distinguished based on the thickness and intensity of Glu and Tyr staining. For TAMRA Aβ internalization IF, neurons were fixed in 4% PFA for 15 min at the indicated times, washed with PBS followed by 0.2% Triton X-100 in PBS for 5 min, blocked, and stained with MAP2 antibody. Images were taken with an LSM 800 confocal microscope using a 40× objective (Plan Apochromat, NA 1.3). Aβ internalization analysis was performed by measuring TAMRA/MAP2 intensity ratios in the nucleus from the middle plane of z stack confocal images. All images were analyzed by Metamorph imaging software and ImageJ software (National Institutes of Health). Ratio measurement of fluorescence intensity in proximal neurites (within 100 µm from the cell body) was performed with the linescan analysis in Metamorph.

Live imaging of MT dynamics and tau dissociation assays

Neurons grown on MatTek dishes were transfected with EB3-EGFP (a gift from F. Polleux) or EB3-tdTomato (a gift from E. Dent, University of Wisconsin, Madison, WI) using Lipofectamine 2000 (Invitrogen). Live-cell imaging of EB3 comets was performed 24–72 h after transfection in complete HBSS media (HBSS, 30 mM glucose, 1 mM $CaCl_2$, 1 mM $MgSO_4$, 4 mM $NaHCO_3$, and 2.5 mM Hepes, pH 7.4) using an epifluorescence microscope (Nikon T*i*) with a controlled temperature and CO_2 incubator. The microscope was equipped with a 100× Plan Apochromat objective (NA 1.45), perfect focus controller, encoded XY stage, filter wheels, and fiber optic–coupled epifluorescence illumination. Videos were acquired with an iXon + DU888 electron-multiplying charge-coupled device camera (Andor Technology) and integrated Nikon Elements software at 2–3 s/frame for 3 min. To better visualize the comets and reduce background, the mean projection of each time-lapse was subtracted from each frame. Kymographs were generated by drawing a region from the cell body to the end of each selected neurite using Metamorph software. Proximal axons and dendrites (within 100 µm from the cell body) were distinguished based on neurite width and length and anterograde movement of all EB3 comets in axons. Parameters describing MT dynamics were defined as follows: rescue/nucleation frequency, number of rescue or nucleation events per μm^2 per min; catastrophe frequency, number of full tracks/total duration of growth; comet density, number of comets per μm^2 per min; growth length, comet movement length in µm; comet lifetime, duration of growth; and growth rate, growth length/comet lifetime (Stepanova et al., 2010). To observe tau dynamics relative to MTs, NIH3T3 cells grown on MatTek dishes were cotransfected with RFP-tubulin and EGFP-tau2N4R WT or S262A mutant by Lipofectamine and PLUS reagent (Invitrogen). Live-cell imaging was performed 24–48 h after transfection in recording media (MEM amino acids and HBSS, 1% penicillin/streptomycin, 25 mM glucose, 4 mM glutamine, 2 µM sodium pyruvate, and 20 mM Hepes, pH 7.4) using epifluorescence microscopy (Nikon T*i*). Each dual-channel time-lapse was recorded at 5 s/frame for 5 min before and 5 min after 10 nM taxol treatment.

MT stability assays

Neurons were treated with Aβ for 1.5 h before addition of 0.2 µg/ml nocodazole for 1 h. At the end of the incubation time, cells were gently washed with warm PHEM buffer (60 mM Pipes, 25 mM Hepes, 10 mM EGTA, and 4 mM $MgCl_2$, pH 6.9) once before extraction with PHEM buffer supplemented with 0.05% Triton X-100, protease inhibitor cocktail, and 10 µM taxol. After 1.5 min at 37°C, a matching volume of 2× fixative buffer (8% PFA and 0.2% glutaraldehyde in 1× PHEM) was added dropwise to the coverslips, and then cells were incubated for another 30 min at 37°C. Neurons were finally washed with TBS and processed for IF labeling. All images were analyzed using ImageJ software by measuring the mean intensity of major proximal neurites (within 100 µm from the cell body). Data are mean βIII-tubulin levels expressed as percentages of vehicle control ± SEM.

Dendritic spine loss assays

Neurons were fixed with 4% PFA for 15 min at room temperature and washed three times with 1× PBS before DiOlistic labeling to define neuronal architecture using the Helios gene gun system (Bio-Rad Laboratories) according to the manufacturer's instructions. Coverslips were mounted in ProLong Gold antifade reagent (Invitrogen) and imaged the next day using an Olympus IX83 microscope with the widefield and disk-scanning unit spinning-disk imaging mentioned in the IF microscopy and analyses section. Z stack images were taken at 0.2-µm step length for 15–20 stacks and shown as maximum projections. Spine density and morphology analysis was performed automatically using NeuronStudio software (Rodriguez et al., 2003). More than 10 neurons (>50 proximal dendritic segments within 100 µm from the cell body) per condition were imaged and analyzed.

Mitochondria motility assays

Neurons were transfected at 9 DIV with Mito-DsRed2 (provided by F. Polleux) using Lipofectamine 2000 and imaged 24 h later using an epifluorescence microscope (Nikon T*i*) equipped with a controlled temperature and CO_2 incubator. Neurons were infected with scr/mDia1 lentiviruses at 6 DIV before 200 nM Aβ for 6 h was added at 10 DIV. Proximal axons (within 100 µm from the cell body) were selected based on length, and videos were acquired at 10 s/frame for 30 min. Mitochondria motility was quantified automatically using particle analysis for each frame, and kymograph analysis was done in ImageJ.

Extracellular fields recordings

Brains were quickly removed from mice sacrificed by cervical dislocation and placed in cold artificial cerebrospinal fluid (ACSF; bubbled with 95% O_2/5% CO_2) containing 124 mM NaCl, 4 mM KCl, 1 mM Na_2HPO_4, 25 mM $NaHCO_3$, 2 mM $CaCl_2$, 2 mM $MgCl_2$, and 10 mM glucose. The pH and osmolarity of the solution were 7.4 and 310 mOsm/liter, respectively. The hippocampi were isolated and placed on a mechanical tissue chopper to produce transverse hippocampal slices of 400 µm thickness. Slices were maintained in a humidified interface chamber at 29°C and continuously perfused (~1 ml/min) with 95% O_2/5% CO_2–bubbled ACSF. Slices were allowed to recover for at least 90 min before beginning the experiment. For recordings, glass electrodes were filled with ACSF and positioned in the CA1 stratum radiatum to record field excitory postsynaptic potentials (fEPSPs) evoked by local stimulation (0.1 ms) of Schaffer collateral fibers using a bipolar concentric electrode placed laterally to the recording electrode (~150 µm). Extracellular responses were acquired using Clampex software (Molecular Devices) and a microamplifier (IE-210; Warner Instruments). The voltage intensity of the stimulation test pulse (square pulse; 100-µs duration) for each slice was determined to be the voltage intensity that had generated 30–40% of the maximum slope obtained using input–output relationships. For LTP, a test pulse was applied every minute. After a steady baseline of 15 min, potentiation was induced with 3 theta-burst stimulations (15-s interval), each one

involving a single train of 10 bursts at 5 Hz, where each burst was composed of four pulses at 100 Hz. The fEPSP slopes after tetanic stimulation were normalized to the mean of the slopes of the fEPSPs acquired during the baseline.

Whole-cell recordings in cultured neurons

For cultured cell recording, rat primary hippocampal neurons (21 DIV, 1 wk after lentiviral infection) were used for tight-seal conventional whole-cell patch clamp. Coverslips were placed in a recording chamber with bath solution containing 119 mM NaCl, 5 mM KCl, 20 mM Hepes, 30 mM glucose, 2 mM $CaCl_2$, 2 mM $MgCl_2$, 100 µM picrotoxin, and 1 µM tetrodotoxin. The pH and osmolarity of the bath solution were adjusted to 7.3 and 330 mOsm/liter, respectively. After acquisition of electrical access, cells were held in voltage-clamp mode at −70 mV for at least 10 min to ensure complete dialysis of the cell with the pipette solution. All the cells were recorded at −70 mV for 10 min, and a 5-mV hyperpolarizing test pulse was applied periodically during recordings to ensure that the access resistance did not change significantly and was <25 MΩ. If so, the recordings were discarded. Signals were filtered at 2 kHz, digitized at 10 kHz, stored, and analyzed offline using MiniAnalysis Software (Version 6.0.7; Synaptosoft). The threshold for event detection was set at 5 pA. Recordings were performed at room temperature under constant perfusion (2 ml/min) and acquired using Clampex software and a microamplifier (MultiClamp 700B; Molecular Devices). For mEPSCs, glass pipettes were filled with intracellular electrode solution (285 mOsm/liter, pH 7.3) containing 130 mM K-gluconate, 10 mM KCl, 10 mM Hepes, 1 mM $MgCl_2$, 0.06 mM $CaCl_2$, 0.1 mM EGTA, 4 mM MgATP, 0.3 mM Na_2GTP, and typically registered with 4–8-MΩ pipette resistances.

Statistical analyses

Data are shown as means ± SEM from at least three independent experiments. For sample sizes ≥5, data were normally distributed from a Kolmogorov–Smirnov normality test and then analyzed by parametric statistical tests. For sample sizes <5, data distribution was assumed to be normal, but this was not formally tested. Statistical analysis between two groups was performed using Student's *t* tests. Comparison among three or more groups was performed using one-way ANOVA with Tukey's post hoc test or Dunnett's multiple comparisons test. Statistical significance was set for $P < 0.05$.

Online supplemental material

Fig. S1 shows additional MT dynamics parameters from measurements of EB3-EGFP comets in dendrites and axons of hippocampal neurons treated with a single dose of Aβ. Fig. S2 shows dose- and time-dependent effects of SMIFH2 on MT stability in WT or tau-KO hippocampal neurons as well as MT dynamics and Aβ internalization in WT hippocampal neurons. Fig. S3 shows the effects of SMIFH2 on steady-state and Aβ or LPA-induced levels of stable MTs in NIH3T3 cells. Fig. S4 shows additional MT dynamics parameters from measurements of EB3-EGFP in dendrites of hippocampal neurons knocked down of mDia1 and describes how FHOD1 depletion fails to affect MT stability and dynamics in 21 DIV hippocampal neurons. Fig. S5 shows dose- and time-dependent effects of SMIFH2 on tau phosphorylation in hippocampal neurons.

Acknowledgments

We thank Franck Polleux for EB3-EGFP and mito-DsRed2 constructs, tau-KO mice, and for helpful discussions; Luciano D'Adamio for APP-KO mice; Ottavio Arancio and Ellen Ezratty for sharing electrophysiology equipment and the confocal microscope, respectively; Jeremy Dargos, Mathilde Gagliardini, Sara Pierre, and Ridwan Sharkar for helping with the conduction of experiments and data analysis; and Ismael Santa-Maria and Roger Lefort for sharing antibody reagents.

This project was funded by a grant from the BrightFocus Foundation (A2015508S) to F. Bartolini and an R01 grant from National Institutes of Health/National Institute on Aging (AG050658-01A1) to F. Bartolini.

The authors declare no competing financial interests.

Author contributions: X. Qu and F. Bartolini conceived the project. X. Qu, F.N. Yuan, C. Corona, S. Pasini, and M.E. Pero conducted and analyzed the experiments. M.L. Shelanski and G.G. Gundersen contributed key reagents, special equipment, and advice. X. Qu and F. Bartolini wrote the manuscript.

Submitted: 5 January 2017
Revised: 15 June 2017
Accepted: 26 July 2017

References

Alvarez, G., J.R. Muñoz-Montaño, J. Satrústegui, J. Avila, E. Bogónez, and J. Díaz-Nido. 1999. Lithium protects cultured neurons against β-amyloid-induced neurodegeneration. *FEBS Lett.* 453:260–264. http://dx.doi.org/10.1016/S0014-5793(99)00685-7

Atarod, D., G. Eskandari-Sedighi, F. Pazhoohi, S.M. Karimian, M. Khajeloo, and G.H. Riazi. 2015. Microtubule dynamicity is more important than stability in memory formation: an in vivo study. *J. Mol. Neurosci.* 56:313–319. http://dx.doi.org/10.1007/s12031-015-0535-4

Baas, P.W., A.N. Rao, A.J. Matamoros, and L. Leo. 2016. Stability properties of neuronal microtubules. *Cytoskeleton (Hoboken).* 73:442–460. http://dx.doi.org/10.1002/cm.21286

Ballatore, C., K.R. Brunden, J.Q. Trojanowski, V.M. Lee, and A.B. Smith III. 2017. Non-naturally occurring small molecule microtubule-stabilizing agents: A potential tactic for CNS-directed therapies. *ACS Chem. Neurosci.* 8:5–7. http://dx.doi.org/10.1021/acschemneuro.6b00384

Bartolini, F., and G.G. Gundersen. 2010. Formins and microtubules. *Biochim. Biophys. Acta.* 1803:164–173. http://dx.doi.org/10.1016/j.bbamcr.2009.07.006

Bartolini, F., J.B. Moseley, J. Schmoranzer, L. Cassimeris, B.L. Goode, and G.G. Gundersen. 2008. The formin mDia2 stabilizes microtubules independently of its actin nucleation activity. *J. Cell Biol.* 181:523–536. http://dx.doi.org/10.1083/jcb.200709029

Bartolini, F., L. Andres-Delgado, X. Qu, S. Nik, N. Ramalingam, L. Kremer, M.A. Alonso, and G.G. Gundersen. 2016. An mDia1-INF2 formin activation cascade facilitated by IQGAP1 regulates stable microtubules in migrating cells. *Mol. Biol. Cell.* 27:1797–1808. http://dx.doi.org/10.1091/mbc.E15-07-0489

Bertrand, J., V. Plouffe, P. Sénéchal, and N. Leclerc. 2010. The pattern of human tau phosphorylation is the result of priming and feedback events in primary hippocampal neurons. *Neuroscience.* 168:323–334. http://dx.doi.org/10.1016/j.neuroscience.2010.04.009

Bieling, P., S. Kandels-Lewis, I.A. Telley, J. van Dijk, C. Janke, and T. Surrey. 2008. CLIP-170 tracks growing microtubule ends by dynamically recognizing composite EB1/tubulin-binding sites. *J. Cell Biol.* 183:1223–1233. http://dx.doi.org/10.1083/jcb.200809190

Biernat, J., N. Gustke, G. Drewes, E.M. Mandelkow, and E. Mandelkow. 1993. Phosphorylation of Ser^{262} strongly reduces binding of tau to microtubules: Distinction between PHF-like immunoreactivity and microtubule binding. *Neuron.* 11:153–163. http://dx.doi.org/10.1016/0896-6273(93)90279-Z

Brandt, D.T., S. Marion, G. Griffiths, T. Watanabe, K. Kaibuchi, and R. Grosse. 2007. Dia1 and IQGAP1 interact in cell migration and phagocytic cup formation. *J. Cell Biol.* 178:193–200. http://dx.doi.org/10.1083/jcb.200612071

Brion, J.P., J.N. Octave, and A.M. Couck. 1994. Distribution of the phosphorylated microtubule-associated protein tau in developing cortical neurons. *Neuroscience.* 63:895–909. http://dx.doi.org/10.1016/0306-4522(94)90533-9

Brunden, K.R., B. Zhang, J. Carroll, Y. Yao, J.S. Potuzak, A.M. Hogan, M. Iba, M.J. James, S.X. Xie, C. Ballatore, et al. 2010. Epothilone D improves microtubule density, axonal integrity, and cognition in a transgenic mouse model of tauopathy. *J. Neurosci.* 30:13861–13866. http://dx.doi.org/10.1523/JNEUROSCI.3059-10.2010

Busciglio, J., A. Lorenzo, J. Yeh, and B.A. Yankner. 1995. β-Amyloid fibrils induce tau phosphorylation and loss of microtubule binding. *Neuron.* 14:879–888. http://dx.doi.org/10.1016/0896-6273(95)90232-5

Chacon, P.J., R. Garcia-Mejias, and A. Rodriguez-Tebar. 2011. Inhibition of RhoA GTPase and the subsequent activation of PTP1B protects cultured hippocampal neurons against amyloid β toxicity. *Mol. Neurodegener.* 6:14. http://dx.doi.org/10.1186/1750-1326-6-14

Chakraborti, S., K. Natarajan, J. Curiel, C. Janke, and J. Liu. 2016. The emerging role of the tubulin code: From the tubulin molecule to neuronal function and disease. *Cytoskeleton (Hoboken).* 73:521–550. http://dx.doi.org/10.1002/cm.21290

Chesarone, M.A., A.G. DuPage, and B.L. Goode. 2010. Unleashing formins to remodel the actin and microtubule cytoskeletons. *Nat. Rev. Mol. Cell Biol.* 11:62–74. http://dx.doi.org/10.1038/nrm2816

Colucci-Guyon, E., F. Niedergang, B.J. Wallar, J. Peng, A.S. Alberts, and P. Chavrier. 2005. A role for mammalian diaphanous-related formins in complement receptor (CR3)-mediated phagocytosis in macrophages. *Curr. Biol.* 15:2007–2012. http://dx.doi.org/10.1016/j.cub.2005.09.051

Cook, T.A., T. Nagasaki, and G.G. Gundersen. 1998. Rho guanosine triphosphatase mediates the selective stabilization of microtubules induced by lysophosphatidic acid. *J. Cell Biol.* 141:175–185. http://dx.doi.org/10.1083/jcb.141.1.175

Dawson, H.N., A. Ferreira, M.V. Eyster, N. Ghoshal, L.I. Binder, and M.P. Vitek. 2001. Inhibition of neuronal maturation in primary hippocampal neurons from τ deficient mice. *J. Cell Sci.* 114:1179–1187.

Deguchi, Y., M. Harada, R. Shinohara, M. Lazarus, Y. Cherasse, Y. Urade, D. Yamada, M. Sekiguchi, D. Watanabe, T. Furuyashiki, and S. Narumiya. 2016. mDia and ROCK mediate actin-dependent presynaptic remodeling regulating synaptic efficacy and anxiety. *Cell Reports.* 17:2405–2417. http://dx.doi.org/10.1016/j.celrep.2016.10.088

Dent, E.W., E.B. Merriam, and X. Hu. 2011. The dynamic cytoskeleton: backbone of dendritic spine plasticity. *Curr. Opin. Neurobiol.* 21:175–181. http://dx.doi.org/10.1016/j.conb.2010.08.013

Derry, W.B., L. Wilson, and M.A. Jordan. 1995. Substoichiometric binding of taxol suppresses microtubule dynamics. *Biochemistry.* 34:2203–2211. http://dx.doi.org/10.1021/bi00007a014

Fanara, P., K.H. Husted, K. Selle, P.Y. Wong, J. Banerjee, R. Brandt, and M.K. Hellerstein. 2010. Changes in microtubule turnover accompany synaptic plasticity and memory formation in response to contextual fear conditioning in mice. *Neuroscience.* 168:167–178. http://dx.doi.org/10.1016/j.neuroscience.2010.03.031

Fischer, D., M.D. Mukrasch, J. Biernat, S. Bibow, M. Blackledge, C. Griesinger, E. Mandelkow, and M. Zweckstetter. 2009. Conformational changes specific for pseudophosphorylation at serine 262 selectively impair binding of tau to microtubules. *Biochemistry.* 48:10047–10055. http://dx.doi.org/10.1021/bi901090m

Fogel, H., S. Frere, O. Segev, S. Bharill, I. Shapira, N. Gazit, T. O'Malley, E. Slomowitz, Y. Berdichevsky, D.M. Walsh, et al. 2014. APP homodimers transduce an amyloid-β-mediated increase in release probability at excitatory synapses. *Cell Reports.* 7:1560–1576. http://dx.doi.org/10.1016/j.celrep.2014.04.024

Ganguly, A., Y. Tang, L. Wang, K. Ladt, J. Loi, B. Dargent, C. Leterrier, and S. Roy. 2015. A dynamic formin-dependent deep F-actin network in axons. *J. Cell Biol.* 210:401–417. http://dx.doi.org/10.1083/jcb.201506110

Goulimari, P., T.M. Kitzing, H. Knieling, D.T. Brandt, S. Offermanns, and R. Grosse. 2005. Gα12/13 is essential for directed cell migration and localized Rho-Dia1 function. *J. Biol. Chem.* 280:42242–42251. http://dx.doi.org/10.1074/jbc.M508690200

Gu, J., B.L. Firestein, and J.Q. Zheng. 2008. Microtubules in dendritic spine development. *J. Neurosci.* 28:12120–12124. http://dx.doi.org/10.1523/JNEUROSCI.2509-08.2008

Gundersen, G.G., M.H. Kalnoski, and J.C. Bulinski. 1984. Distinct populations of microtubules: Tyrosinated and nontyrosinated alpha tubulin are distributed differently in vivo. *Cell.* 38:779–789. http://dx.doi.org/10.1016/0092-8674(84)90273-3

Harada, A., K. Oguchi, S. Okabe, J. Kuno, S. Terada, T. Ohshima, R. Sato-Yoshitake, Y. Takei, T. Noda, and N. Hirokawa. 1994. Altered microtubule organization in small-calibre axons of mice lacking *tau* protein. *Nature.* 369:488–491. http://dx.doi.org/10.1038/369488a0

Honnappa, S., O. Okhrimenko, R. Jaussi, H. Jawhari, I. Jelesarov, F.K. Winkler, and M.O. Steinmetz. 2006. Key interaction modes of dynamic +TIP networks. *Mol. Cell.* 23:663–671. http://dx.doi.org/10.1016/j.molcel.2006.07.013

Hoover, B.R., M.N. Reed, J. Su, R.D. Penrod, L.A. Kotilinek, M.K. Grant, R. Pitstick, G.A. Carlson, L.M. Lanier, L.L. Yuan, et al. 2010. Tau mislocalization to dendritic spines mediates synaptic dysfunction independently of neurodegeneration. *Neuron.* 68:1067–1081. http://dx.doi.org/10.1016/j.neuron.2010.11.030

Hotulainen, P., O. Llano, S. Smirnov, K. Tanhuanpää, J. Faix, C. Rivera, and P. Lappalainen. 2009. Defining mechanisms of actin polymerization and depolymerization during dendritic spine morphogenesis. *J. Cell Biol.* 185:323–339. http://dx.doi.org/10.1083/jcb.200809046

Hu, X., L. Ballo, L. Pietila, C. Viesselmann, J. Ballweg, D. Lumbard, M. Stevenson, E. Merriam, and E.W. Dent. 2011. BDNF-induced increase of PSD-95 in dendritic spines requires dynamic microtubule invasions. *J. Neurosci.* 31:15597–15603. http://dx.doi.org/10.1523/JNEUROSCI.2445-11.2011

Huesa, G., M.A. Baltrons, P. Gómez-Ramos, A. Morán, A. García, J. Hidalgo, S. Francés, G. Santpere, I. Ferrer, and E. Galea. 2010. Altered distribution of RhoA in Alzheimer's disease and AβPP overexpressing mice. *J. Alzheimers Dis.* 19:37–56. http://dx.doi.org/10.3233/JAD-2010-1203

Ittner, L.M., and J. Götz. 2011. Amyloid-β and tau—a toxic *pas de deux* in Alzheimer's disease. *Nat. Rev. Neurosci.* 12:65–72. http://dx.doi.org/10.1038/nrn2967

Ittner, L.M., Y.D. Ke, F. Delerue, M. Bi, A. Gladbach, J. van Eersel, H. Wölfing, B.C. Chieng, M.J. Christie, I.A. Napier, et al. 2010. Dendritic function of tau mediates amyloid-β toxicity in Alzheimer's disease mouse models. *Cell.* 142:387–397. http://dx.doi.org/10.1016/j.cell.2010.06.036

Janke, C. 2014. The tubulin code: Molecular components, readout mechanisms, and functions. *J. Cell Biol.* 206:461–472. http://dx.doi.org/10.1083/jcb.201406055

Janke, C., and J.C. Bulinski. 2011. Post-translational regulation of the microtubule cytoskeleton: mechanisms and functions. *Nat. Rev. Mol. Cell Biol.* 12:773–786. http://dx.doi.org/10.1038/nrm3227

Janke, C., and M. Kneussel. 2010. Tubulin post-translational modifications: encoding functions on the neuronal microtubule cytoskeleton. *Trends Neurosci.* 33:362–372. http://dx.doi.org/10.1016/j.tins.2010.05.001

Jaworski, J., L.C. Kapitein, S.M. Gouveia, B.R. Dortland, P.S. Wulf, I. Grigoriev, P. Camera, S.A. Spangler, P. Di Stefano, J. Demmers, et al. 2009. Dynamic microtubules regulate dendritic spine morphology and synaptic plasticity. *Neuron.* 61:85–100. http://dx.doi.org/10.1016/j.neuron.2008.11.013

Jin, M., N. Shepardson, T. Yang, G. Chen, D. Walsh, and D.J. Selkoe. 2011. Soluble amyloid β-protein dimers isolated from Alzheimer cortex directly induce Tau hyperphosphorylation and neuritic degeneration. *Proc. Natl. Acad. Sci. USA.* 108:5819–5824. http://dx.doi.org/10.1073/pnas.1017033108

Kadavath, H., R.V. Hofele, J. Biernat, S. Kumar, K. Tepper, H. Urlaub, E. Mandelkow, and M. Zweckstetter. 2015. Tau stabilizes microtubules by binding at the interface between tubulin heterodimers. *Proc. Natl. Acad. Sci. USA.* 112:7501–7506. http://dx.doi.org/10.1073/pnas.1504081112

Kapitein, L.C., K.W. Yau, and C.C. Hoogenraad. 2010. Microtubule dynamics in dendritic spines. *Methods Cell Biol.* 97:111–132. http://dx.doi.org/10.1016/S0091-679X(10)97007-6

Kapitein, L.C., K.W. Yau, S.M. Gouveia, W.A. van der Zwan, P.S. Wulf, N. Keijzer, J. Demmers, J. Jaworski, A. Akhmanova, and C.C. Hoogenraad. 2011. NMDA receptor activation suppresses microtubule growth and spine entry. *J. Neurosci.* 31:8194–8209. http://dx.doi.org/10.1523/JNEUROSCI.6215-10.2011

Kaul, N., V. Soppina, and K.J. Verhey. 2014. Effects of α-tubulin K40 acetylation and detyrosination on kinesin-1 motility in a purified system. *Biophys. J.* 106:2636–2643. http://dx.doi.org/10.1016/j.bpj.2014.05.008

Konishi, Y., and M. Setou. 2009. Tubulin tyrosination navigates the kinesin-1 motor domain to axons. *Nat. Neurosci.* 12:559–567. http://dx.doi.org/10.1038/nn.2314

Kreitzer, G., G. Liao, and G.G. Gundersen. 1999. Detyrosination of tubulin regulates the interaction of intermediate filaments with microtubules in vivo via a kinesin-dependent mechanism. *Mol. Biol. Cell.* 10:1105–1118. http://dx.doi.org/10.1091/mbc.10.4.1105

Lacroix, B., J. van Dijk, N.D. Gold, J. Guizetti, G. Aldrian-Herrada, K. Rogowski, D.W. Gerlich, and C. Janke. 2010. Tubulin polyglutamylation stimulates spastin-mediated microtubule severing. *J. Cell Biol.* 189:945–954. http://dx.doi.org/10.1083/jcb.201001024

LaFerla, F.M. 2010. Pathways linking Aβ and tau pathologies. *Biochem. Soc. Trans.* 38:993–995. http://dx.doi.org/10.1042/BST0380993

Law, R., T. Dixon-Salazar, J. Jerber, N. Cai, A.A. Abbasi, M.S. Zaki, K. Mittal, S.B. Gabriel, M.A. Rafiq, V. Khan, et al. 2014. Biallelic truncating mutations in FMN2, encoding the actin-regulatory protein Formin 2, cause nonsyndromic autosomal-recessive intellectual disability. *Am. J. Hum. Genet.* 95:721–728. http://dx.doi.org/10.1016/j.ajhg.2014.10.016

Lee, G., S.T. Newman, D.L. Gard, H. Band, and G. Panchamoorthy. 1998. Tau interacts with src-family non-receptor tyrosine kinases. *J. Cell Sci.* 111:3167–3177.

Lefort, R., J. Pozueta, and M. Shelanski. 2012. Cross-linking of cell surface amyloid precursor protein leads to increased β-amyloid peptide production in hippocampal neurons: Implications for Alzheimer's disease. *J. Neurosci.* 32:10674–10685. http://dx.doi.org/10.1523/JNEUROSCI.6473-11.2012

Leo, L., W. Yu, M. D'Rozario, E.A. Waddell, D.R. Marenda, M.A. Baird, M.W. Davidson, B. Zhou, B. Wu, L. Baker, et al. 2015. Vertebrate fidgetin restrains axonal growth by severing labile domains of microtubules. *Cell Reports.* 12:1723–1730. http://dx.doi.org/10.1016/j.celrep.2015.08.017

Lepicard, S., B. Franco, F. de Bock, and M.L. Parmentier. 2014. A presynaptic role of microtubule-associated protein 1/Futsch in *Drosophila*: Regulation of active zone number and neurotransmitter release. *J. Neurosci.* 34:6759–6771. http://dx.doi.org/10.1523/JNEUROSCI.4282-13.2014

Lewkowicz, E., F. Herit, C. Le Clainche, P. Bourdoncle, F. Perez, and F. Niedergang. 2008. The microtubule-binding protein CLIP-170 coordinates mDia1 and actin reorganization during CR3-mediated phagocytosis. *J. Cell Biol.* 183:1287–1298. http://dx.doi.org/10.1083/jcb.200807023

Liu, J., S. Pasini, M.L. Shelanski, and L.A. Greene. 2014. Activating transcription factor 4 (ATF4) modulates post-synaptic development and dendritic spine morphology. *Front. Cell. Neurosci.* 8:177. http://dx.doi.org/10.3389/fncel.2014.00177

Lu, R., H. Wang, Z. Liang, L. Ku. W.T. O'Donnell, W. Li, S.T. Warren, and Y. Feng. 2004. The fragile X protein controls microtubule-associated protein 1B translation and microtubule stability in brain neuron development. *Proc. Natl. Acad. Sci. USA.* 101:15201–15206.

Maas, C., D. Belgardt, H.K. Lee, F.F. Heisler, C. Lappe-Siefke, M.M. Magiera, J. van Dijk, T.J. Hausrat, C. Janke, and M. Kneussel. 2009. Synaptic activation modifies microtubules underlying transport of postsynaptic cargo. *Proc. Natl. Acad. Sci. USA.* 106:8731–8736. http://dx.doi.org/10.1073/pnas.0812391106

Mairet-Coello, G., J. Courchet, S. Pieraut, V. Courchet, A. Maximov, and F. Polleux. 2013. The CAMKK2-AMPK kinase pathway mediates the synaptotoxic effects of Aβ oligomers through Tau phosphorylation. *Neuron.* 78:94–108. http://dx.doi.org/10.1016/j.neuron.2013.02.003

Matamoros, A.J., and P.W. Baas. 2016. Microtubules in health and degenerative disease of the nervous system. *Brain Res. Bull.* 126:217–225. http://dx.doi.org/10.1016/j.brainresbull.2016.06.016

McKenney, R.J., W. Huynh, R.D. Vale, and M. Sirajuddin. 2016. Tyrosination of α-tubulin controls the initiation of processive dynein-dynactin motility. *EMBO J.* 35:1175–1185. http://dx.doi.org/10.15252/embj.201593071

McVicker, D.P., A.M. Awe, K.E. Richters, R.L. Wilson, D.A. Cowdrey, X. Hu, E.R. Chapman, and E.W. Dent. 2016. Transport of a kinesin-cargo pair along microtubules into dendritic spines undergoing synaptic plasticity. *Nat. Commun.* 7:12741. http://dx.doi.org/10.1038/ncomms12741

Merriam, E.B., D.C. Lumbard, C. Viesselmann, J. Ballweg, M. Stevenson, L. Pietila, X. Hu, and E.W. Dent. 2011. Dynamic microtubules promote synaptic NMDA receptor-dependent spine enlargement. *PLoS One.* 6:e27688. http://dx.doi.org/10.1371/journal.pone.0027688

Merriam, E.B., M. Millette, D.C. Lumbard, W. Saengsawang, T. Fothergill, X. Hu, L. Ferhat, and E.W. Dent. 2013. Synaptic regulation of microtubule dynamics in dendritic spines by calcium, F-actin, and drebrin. *J. Neurosci.* 33:16471–16482. http://dx.doi.org/10.1523/JNEUROSCI.0661-13.2013

Mitsuyama, F., G. Niimi, K. Kato, K. Hirosawa, K. Mikoshiba, M. Okuya, K. Karagiozov, Y. Kato, T. Kanno, H. Sanoe, and T. Koide. 2008. Redistribution of microtubules in dendrites of hippocampal CA1 neurons after tetanic stimulation during long-term potentiation. *Ital. J. Anat. Embryol.* 113:17–27.

Muhia, M., E. Thies, D. Labonté, A.E. Ghiretti, K.V. Gromova, F. Xompero, C. Lappe-Siefke, I. Hermans-Borgmeyer, D. Kuhl, M. Schweizer, et al. 2016. The kinesin KIF21B regulates microtubule dynamics and is essential for neuronal morphology, synapse function, and learning and memory. *Cell Reports.* 15:968–977. http://dx.doi.org/10.1016/j.celrep.2016.03.086

Muratore, C.R., H.C. Rice, P. Srikanth, D.G. Callahan, T. Shin, L.N. Benjamin, D.M. Walsh, D.J. Selkoe, and T.L. Young-Pearse. 2014. The familial Alzheimer's disease APPV717I mutation alters APP processing and Tau expression in iPSC-derived neurons. *Hum. Mol. Genet.* 23:3523–3536. http://dx.doi.org/10.1093/hmg/ddu064

Nimmrich, V., and U. Ebert. 2009. Is Alzheimer's disease a result of presynaptic failure? Synaptic dysfunctions induced by oligomeric beta-amyloid. *Rev. Neurosci.* 20:1–12. http://dx.doi.org/10.1515/REVNEURO.2009.20.1.1

Nirschl, J.J., M.M. Magiera, J.E. Lazarus, C. Janke, and E.L. Holzbaur. 2016. α-Tubulin tyrosination and CLIP-170 phosphorylation regulate the initiation of dynein-driven transport in neurons. *Cell Reports.* 14:2637–2652. http://dx.doi.org/10.1016/j.celrep.2016.02.046

Palazzo, A.F., T.A. Cook, A.S. Alberts, and G.G. Gundersen. 2001. mDia mediates Rho-regulated formation and orientation of stable microtubules. *Nat. Cell Biol.* 3:723–729. http://dx.doi.org/10.1038/35087035

Palazzo, A.F., C.H. Eng, D.D. Schlaepfer, E.E. Marcantonio, and G.G. Gundersen. 2004. Localized stabilization of microtubules by integrin- and FAK-facilitated Rho signaling. *Science.* 303:836–839. http://dx.doi.org/10.1126/science.1091325

Pawson, C., B.A. Eaton, and G.W. Davis. 2008. Formin-dependent synaptic growth: Evidence that Dlar signals via Diaphanous to modulate synaptic actin and dynamic pioneer microtubules. *J. Neurosci.* 28:11111–11123. http://dx.doi.org/10.1523/JNEUROSCI.0833-08.2008

Penazzi, L., C. Tackenberg, A. Ghori, N. Golovyashkina, B. Niewidok, K. Selle, C. Ballatore, A.B. Smith III, L. Bakota, and R. Brandt. 2016. Aβ-mediated spine changes in the hippocampus are microtubule-dependent and can be reversed by a subnanomolar concentration of the microtubule-stabilizing agent epothilone D. *Neuropharmacology.* 105:84–95. http://dx.doi.org/10.1016/j.neuropharm.2016.01.002

Peris, L., M. Thery, J. Fauré, Y. Saoudi, L. Lafanechère, J.K. Chilton, P. Gordon-Weeks, N. Galjart, M. Bornens, L. Wordeman, et al. 2006. Tubulin tyrosination is a major factor affecting the recruitment of CAP-Gly proteins at microtubule plus ends. *J. Cell Biol.* 174:839–849. http://dx.doi.org/10.1083/jcb.200512058

Peris, L., M. Wagenbach, L. Lafanechère, J. Brocard, A.T. Moore, F. Kozielski, D. Job, L. Wordeman, and A. Andrieux. 2009. Motor-dependent microtubule disassembly driven by tubulin tyrosination. *J. Cell Biol.* 185:1159–1166. http://dx.doi.org/10.1083/jcb.200902142

Pianu, B., R. Lefort, L. Thuiliere, E. Tabourier, and F. Bartolini. 2014. The $A\beta_{1-42}$ peptide regulates microtubule stability independently of tau. *J. Cell Sci.* 127:1117–1127. http://dx.doi.org/10.1242/jcs.143750

Pozueta, J., R. Lefort, and M.L. Shelanski. 2013a. Synaptic changes in Alzheimer's disease and its models. *Neuroscience.* 251:51–65. http://dx.doi.org/10.1016/j.neuroscience.2012.05.050

Pozueta, J., R. Lefort, E.M. Ribe, C.M. Troy, O. Arancio, and M. Shelanski. 2013b. Caspase-2 is required for dendritic spine and behavioural alterations in J20 APP transgenic mice. *Nat. Commun.* 4:1939. http://dx.doi.org/10.1038/ncomms2927

Puzzo, D., R. Piacentini, M. Fá, W. Gulisano, D.D. Li Puma, A. Staniszewski, H. Zhang, M.R. Tropea, S. Cocco, A. Palmeri, et al. 2017. LTP and memory impairment caused by extracellular Aβ and Tau oligomers is APP-dependent. *eLife.* 6:e26911. http://dx.doi.org/10.7554/eLife.26991

Qiang, L., W. Yu, A. Andreadis, M. Luo, and P.W. Baas. 2006. Tau protects microtubules in the axon from severing by katanin. *J. Neurosci.* 26:3120–3129. http://dx.doi.org/10.1523/JNEUROSCI.5392-05.2006

Rapoport, M., H.N. Dawson, L.I. Binder, M.P. Vitek, and A. Ferreira. 2002. Tau is essential to β-amyloid-induced neurotoxicity. *Proc. Natl. Acad. Sci. USA.* 99:6364–6369. http://dx.doi.org/10.1073/pnas.092136199

Rizvi, S.A., E.M. Neidt, J. Cui, Z. Feiger, C.T. Skau, M.L. Gardel, S.A. Kozmin, and D.R. Kovar. 2009. Identification and characterization of a small molecule inhibitor of formin-mediated actin assembly. *Chem. Biol.* 16:1158–1168. http://dx.doi.org/10.1016/j.chembiol.2009.10.006

Roberson, E.D., K. Scearce-Levie, J.J. Palop, F. Yan, I.H. Cheng, T. Wu, H. Gerstein, G.Q. Yu, and L. Mucke. 2007. Reducing endogenous tau ameliorates amyloid β-induced deficits in an Alzheimer's disease mouse model. *Science.* 316:750–754. http://dx.doi.org/10.1126/science.1141736

Rodriguez, A., D. Ehlenberger, K. Kelliher, M. Einstein, S.C. Henderson, J.H. Morrison, P.R. Hof, and S.L. Wearne. 2003. Automated reconstruction of three-dimensional neuronal morphology from laser scanning microscopy images. *Methods.* 30:94–105. http://dx.doi.org/10.1016/S1046-2023(03)00011-2

Rogowski, K., J. van Dijk, M.M. Magiera, C. Bosc, J.C. Deloulme, A. Bosson, L. Peris, N.D. Gold, B. Lacroix, M. Bosch Grau, et al. 2010. A family of protein-deglutamylating enzymes associated with neurodegeneration. *Cell.* 143:564–578. http://dx.doi.org/10.1016/j.cell.2010.10.014

Saganich, M.J., B.E. Schroeder, V. Galvan, D.E. Bredesen, E.H. Koo, and S.F. Heinemann. 2006. Deficits in synaptic transmission and learning in amyloid precursor protein (APP) transgenic mice require C-terminal cleavage of APP. *J. Neurosci.* 26:13428–13436. http://dx.doi.org/10.1523/JNEUROSCI.4180-06.2006

Salomon, S.N., M. Haber, K.K. Murai, and R.J. Dunn. 2008. Localization of the Diaphanous-related formin Daam1 to neuronal dendrites. *Neurosci. Lett.* 447:62–67. http://dx.doi.org/10.1016/j.neulet.2008.09.051

Sherman, M.A., M. LaCroix, F. Amar, M.E. Larson, C. Forster, A. Aguzzi, D.A. Bennett, M. Ramsden, and S.E. Lesné. 2016. Soluble conformers of Aβ and Tau alter selective proteins governing axonal transport. *J. Neurosci.* 36:9647–9658. http://dx.doi.org/10.1523/JNEUROSCI.1899-16.2016

Sirajuddin, M., L.M. Rice, and R.D. Vale. 2014. Regulation of microtubule motors by tubulin isotypes and post-translational modifications. *Nat. Cell Biol.* 16:335–344. http://dx.doi.org/10.1038/ncb2920

Soykan, T., N. Kaempf, T. Sakaba, D. Vollweiter, F. Goerdeler, D. Puchkov, N.L. Kononenko, and V. Haucke. 2017. Synaptic vesicle endocytosis occurs on multiple timescales and is mediated by formin-dependent actin assembly. *Neuron.* 93:854–866.

Stepanova, T., I. Smal, J. van Haren, U. Akinci, Z. Liu, M. Miedema, R. Limpens, M. van Ham, M. van der Reijden, R. Poot, et al. 2010. History-dependent catastrophes regulate axonal microtubule behavior. *Curr. Biol.* 20:1023–1028. http://dx.doi.org/10.1016/j.cub.2010.04.024

Stine, W.B. Jr., K.N. Dahlgren, G.A. Krafft, and M.J. LaDu. 2003. In vitro characterization of conditions for amyloid-β peptide oligomerization and fibrillogenesis. *J. Biol. Chem.* 278:11612–11622. http://dx.doi.org/10.1074/jbc.M210207200

Sudo, H., and P.W. Baas. 2010. Acetylation of microtubules influences their sensitivity to severing by katanin in neurons and fibroblasts. *J. Neurosci.* 30:7215–7226. http://dx.doi.org/10.1523/JNEUROSCI.0048-10.2010

Trotta, N., G. Orso, M.G. Rossetto, A. Daga, and K. Broadie. 2004. The hereditary spastic paraplegia gene, *spastin*, regulates microtubule stability to modulate synaptic structure and function. *Curr. Biol.* 14:1135–1147. http://dx.doi.org/10.1016/j.cub.2004.06.058

Tsushima, H., M. Emanuele, A. Polenghi, A. Esposito, M. Vassalli, A. Barberis, F. Difato, and E. Chieregatti. 2015. HDAC6 and RhoA are novel players in Abeta-driven disruption of neuronal polarity. *Nat. Commun.* 6:7781. http://dx.doi.org/10.1038/ncomms8781

Uchida, S., and G.P. Shumyatsky. 2015. Deceivingly dynamic: Learning-dependent changes in stathmin and microtubules. *Neurobiol. Learn. Mem.* 124:52–61. http://dx.doi.org/10.1016/j.nlm.2015.07.011

Uchida, S., G. Martel, A. Pavlowsky, S. Takizawa, C. Hevi, Y. Watanabe, E.R. Kandel, J.M. Alarcon, and G.P. Shumyatsky. 2014. Learning-induced and stathmin-dependent changes in microtubule stability are critical for memory and disrupted in ageing. *Nat. Commun.* 5:4389. http://dx.doi.org/10.1038/ncomms5389

Vossel, K.A., K. Zhang, J. Brodbeck, A.C. Daub, P. Sharma, S. Finkbeiner, B. Cui, and L. Mucke. 2010. Tau reduction prevents Aβ-induced defects in axonal transport. *Science.* 330:198. http://dx.doi.org/10.1126/science.1194653

Wang, L., T.L. Benzinger, Y. Su, J. Christensen, K. Friedrichsen, P. Aldea, J. McConathy, N.J. Cairns, A.M. Fagan, J.C. Morris, and B.M. Ances. 2016. Evaluation of Tau imaging in staging Alzheimer disease and revealing interactions between β-amyloid and Tauopathy. *JAMA Neurol.* 73:1070–1077. http://dx.doi.org/10.1001/jamaneurol.2016.2078

Xu, Y., J.B. Moseley, I. Sagot, F. Poy, D. Pellman, B.L. Goode, and M.J. Eck. 2004. Crystal structures of a Formin Homology-2 domain reveal a tethered dimer architecture. *Cell.* 116:711–723. http://dx.doi.org/10.1016/S0092-8674(04)00210-7

Zempel, H., E. Thies, E. Mandelkow, and E.M. Mandelkow. 2010. Aβ oligomers cause localized Ca^{2+} elevation, missorting of endogenous Tau into dendrites, Tau phosphorylation, and destruction of microtubules and spines. *J. Neurosci.* 30:11938–11950. http://dx.doi.org/10.1523/JNEUROSCI.2357-10.2010

Zempel, H., J. Luedtke, Y. Kumar, J. Biernat, H. Dawson, E. Mandelkow, and E.M. Mandelkow. 2013. Amyloid-β oligomers induce synaptic damage via Tau-dependent microtubule severing by TTLL6 and spastin. *EMBO J.* 32:2920–2937. http://dx.doi.org/10.1038/emboj.2013.207

Zhang, Y.Q., A.M. Bailey, H.J. Matthies, R.B. Renden, M.A. Smith, S.D. Speese, G.M. Rubin, and K. Broadie. 2001. *Drosophila* fragile X-related gene regulates the MAP1B homolog Futsch to control synaptic structure and function. *Cell.* 107:591–603. http://dx.doi.org/10.1016/S0092-8674(01)00589-X

Zheng, H., M. Jiang, M.E. Trumbauer, D.J. Sirinathsinghji, R. Hopkins, D.W. Smith, R.P. Heavens, G.R. Dawson, S. Boyce, M.W. Conner, et al. 1995. β-Amyloid precursor protein-deficient mice show reactive gliosis and decreased locomotor activity. *Cell.* 81:525–531. http://dx.doi.org/10.1016/0092-8674(95)90073-X

Zheng, W.H., S. Bastianetto, F. Mennicken, W. Ma, and S. Kar. 2002. Amyloid β peptide induces tau phosphorylation and loss of cholinergic neurons in rat primary septal cultures. *Neuroscience.* 115:201–211. http://dx.doi.org/10.1016/S0306-4522(02)00404-9

Zhou, L., J. McInnes, K. Wierda, M. Holt, A.G. Herrmann, R.J. Jackson, Y.C. Wang, J. Swerts, J. Beyens, K. Miskiewicz, et al. 2017. Tau association with synaptic vesicles causes presynaptic dysfunction. *Nat. Commun.* 8:15295. http://dx.doi.org/10.1038/ncomms15295